American Society of Mechanical Engineers

ASME Accepted Manuscript Repository

Institutional Repository Cover Sheet

First Last

ASME Paper Title: Effect of surface curvature on contact resistance between cylinders

Authors: Michael Mayer, Marc Hodes, Toby Kirk and Darren Crowdy

ASME Journal Title: J. Heat Transfer

Volume/Issue _____141_____ Date of Publication (VOR* Online) __4 Feb 2019_____

ASME Digital Collection URL: http://heattransfer.asmedigitalcollection.asme.org/

DOI: 10.1115/1.4042441

*VOR (version of record)

Journal of Heat Transfer. Received July 24, 2018;
Accepted manuscript posted January 08, 2019. doi:10.1115/1.4042441
Copyright (c) 2019 by ASME

Effect of Surface Curvature on Contact Resistance between Cylinders

Michael Mayer*, Marc Hodes†, Toby Kirk‡, and Darren Crowdy§

December 19, 2018

Abstract

Due to the microscopic roughness of contacting materials, an additional thermal resistance arises from the constriction and spreading of heat near contact spots. Predictive models for contact resistance typically consider abutting semi-infinite cylinders subjected to an adiabatic boundary condition along their outer radius. At the nominal plane of contact an isothermal and circular contact spot is surrounded by an adiabatic annulus and the far-field boundary condition is one of constant heat flux. However, cylinders with flat bases do not mimic the geometry of contacts. To remedy this, we perturb the geometry of the problem such that, in cross section, the circular contact is surrounded by an adiabatic arc. When the curvature of this arc is small, we employ a series solution for the leading-order (flat base) problem. Then, Green's second identity is used to compute the increase in spreading resistance in a single cylinder, and thus the contact resistance for abutting ones, without fully resolving the temperature field. Complementary numerical results for contact resistance span the full range of contact fraction and protrusion angle of the arc. The results suggest as much as a 10-15% increase in contact resistance for realistic contact fraction and asperity slopes. When the protrusion angle is negative, the decrease in spreading resistance for a single cylinder is also provided.

1 Introduction

Flux-based thermal resistance, R'', subsequently referred to as thermal resistance, is the temperature drop (ΔT) per unit heat flux (q'') in the direction of heat flow as per

$$R'' = \frac{\Delta T}{q''} \tag{1}$$

In general, it may capture multi-dimensional conduction and convection effects. In the elementary case of one-dimensional, steady-state, Cartesian heat conduction, it is

$$R''_{1\mathrm{D}} = \frac{L}{k} \tag{2}$$

*Department of Mechanical Engineering, Tufts University, Medford, MA, USA, e-mail: michael.mayer@tufts.edu.
†Department of Mechanical Engineering, Tufts University, Medford, MA, USA
‡Mathematical Institute, University of Oxford, Oxford, England
§Department of Mathematics, Imperial College, London, England

Accepted Manuscript Not Copyedited

Downloaded From: https://heattransfer.asmedigitalcollection.asme.org on 01/28/2019 Terms of Use: http://www.asme.org/about-asme/terms-of-use

Journal of Heat Transfer. Received July 24, 2018;
Accepted manuscript posted January 08, 2019. doi:10.1115/1.4042441
Copyright (c) 2019 by ASME

where L is the length of the material through which heat conducts and k is its thermal conductivity. When conduction is multi-dimensional because of the size of the heat source (sink) on a flat base of a domain, the total thermal resistance ($R''_{\rm t}$) is based upon the mean heat flux through it ($\bar{q}''$) and can be decomposed into

$$R''_{\rm t} = R''_{\rm 1D} + R''_{\rm sp} \tag{3}$$

where $R''_{\rm sp}$ is the spreading (constriction) resistance. It accounts for the additional temperature drop due to spreading or constriction of isotherms ($\Delta T_{\rm sp}$) per unit heat flux in the direction of heat flow as per

$$R''_{\rm sp} = \frac{\Delta T_{\rm sp}}{\bar{q}''} \tag{4}$$

where $\Delta T_{\rm sp} = \bar{T}_{\rm s} - \bar{T}_{\rm s,pl}$, where $\bar{T}_{\rm s}$ is the mean temperature of the source (sink) and $\bar{T}_{\rm s,pl}$ that of the plane of the source (sink). The concept of spreading resistance on account of the width of a heat source being smaller than that of a semi-infinite, Cartesian domain for an isoflux source as per a solution by Mikic [1] is illustrated in Fig. 1.

For one-dimensional, steady-state, Cartesian heat transfer between solid materials 1 and 2, in the idealized limit where temperature continuity is imposed across a flat interface between them, i.e., Kapitza resistance is neglected, the thermal resistance ($R''_{\rm ideal}$) is

$$R''_{\rm ideal} = \frac{L_1}{k_1} + \frac{L_2}{k_2} \tag{5}$$

In reality, the thermal resistance to heat transfer though the materials ($R''_{\rm real}$) is

$$R''_{\rm real} = \frac{L_1}{k_1} + \frac{L_2}{k_2} + R''_{\rm tc} \tag{6}$$

where $R''_{\rm tc}$ is the (thermal) contact resistance. It captures the additional resistance to heat transfer that arises due to the roughness of real surfaces. A consequence of the roughness of real surfaces is that, typically, only 1-2% of their projected surface area is in physical contact [2]. Contact occurs only on the the tips of asperities, elsewhere leaving an interspatial gap. As the thermal conductivity of the interspatial fluid (typically air) is generally negligible compared to those of the contacting materials, heat flowing between the two surfaces will constrict and spread near the contacts. This constriction and spreading gives rise to contact resistance, depicted in Fig. 2 as per the solution by Crowdy [3] discussed by Hodes *et al.* [4] in this context for the Cartesian-geometry problem. When the lengths of materials 1 and 2 are large compared to the scale of the pitch of the contacts, as tends to be the case in real systems, contact resistance may be interpreted as a temperature discontinuity at the nominal plane of contact.

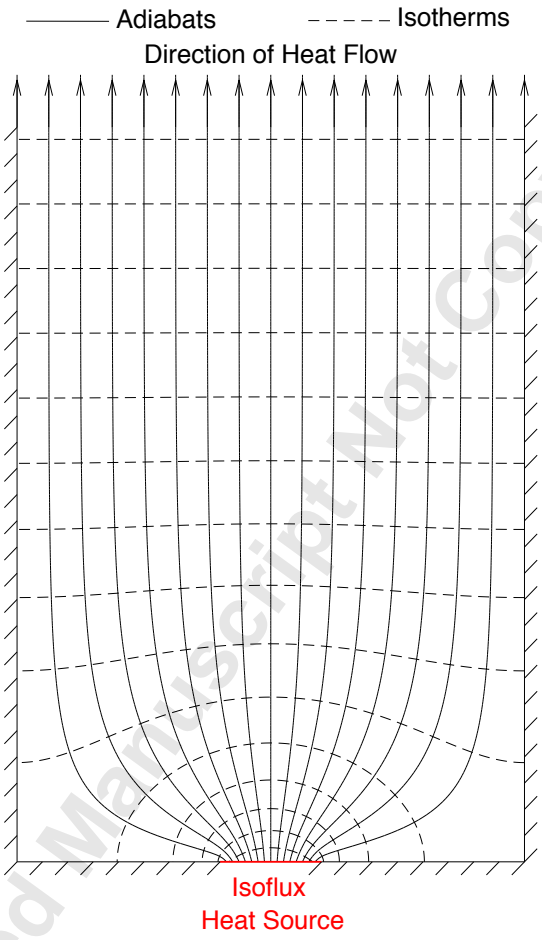
The typical approach to the modeling of contact resistance is to use surface profiles and thermophysical properties of the contacting materials to develop a distribution of contact locations and sizes. This distribution is combined with spreading resistance expressions derived from the modeling of a single contact [5]. Because of this, much research has been done on the modeling of single contacts, our focus here. Considering heat conduction between geometrically-identical contacting materials not necessarily of equal thermal conductivity, it follows from the symmetry arguments discussed in Cooper *et al.* [5] and generalized by Das and Sadhal [6] that the contact regions are isothermal. Thus the contact resistance problem reduces to a spreading resistance one. Decomposing the temperature field in an arbitrary domain with an isothermal contact spot into one-dimensional (1D) and perturbative (p) parts, Eq. (3) becomes

$$\overbrace{\frac{T_{\rm s} - T_\infty}{\bar{q}''}}^{R''_{\rm t}} = \overbrace{\frac{T_{\rm 1D,s} - T_{\rm 1D,\infty}}{\bar{q}''}}^{R''_{\rm 1D}} + \overbrace{\frac{T_{\rm p,s} - T_{\rm p,\infty}}{\bar{q}''}}^{R''_{\rm sp}} \tag{7}$$

Accepted Manuscript Not Copyrighted

Downloaded From: https://heattransfer.asmedigitalcollection.asme.org on 01/28/2019 Terms of Use: http://www.asme.org/about-asme/terms-of-use

Journal of Heat Transfer. Received July 24, 2018;
Accepted manuscript posted January 08, 2019. doi:10.1115/1.4042441
Copyright (c) 2019 by ASME

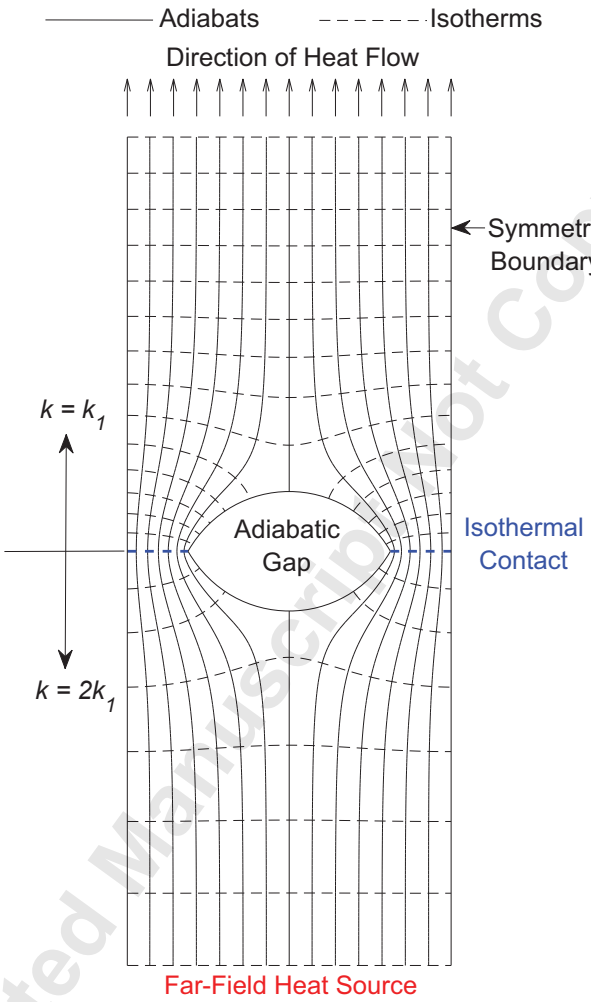


Accepted Manuscript Not Copyedited

Figure 1: Isotherms and adiabats for a two-dimensional temperature field when an isoflux heat source is of smaller width than a semi-infinite, Cartesian domain.

Downloaded From: https://heattransfer.asmedigitalcollection.asme.org on 01/28/2019 Terms of Use: http://www.asme.org/about-asme/terms-of-use

Journal of Heat Transfer. Received July 24, 2018;
Accepted manuscript posted January 08, 2019. doi:10.1115/1.4042441
Copyright (c) 2019 by ASME



Accepted Manuscript Not Copyedited

Figure 2: Illustration of contact resistance in Cartesian-geometry domain with materials of differing conductivities.

Downloaded From: https://heattransfer.asmedigitalcollection.asme.org on 01/28/2019 Terms of Use: http://www.asme.org/about-asme/terms-of-use

Journal of Heat Transfer. Received July 24, 2018;
Accepted manuscript posted January 08, 2019. doi:10.1115/1.4042441
Copyright (c) 2019 by ASME

where the subscripts ∞ and s denote far-field and source temperatures, respectively. Thus,

$$R''_{\mathrm{sp}} = \frac{T_{\mathrm{s}} - T_{\mathrm{1D,s}}}{\bar{q}''} - \frac{T_{\infty} - T_{\mathrm{1D},\infty}}{\bar{q}''} \tag{8}$$

This definition provides a means of calculating the spreading resistance in a contact with arbitrary shape by either specifying a temperature drop and solving for heat flux, or vice versa. As discussed further below, contacts are typically modeled with a flat base and an isothermal contact spot. Then, by choosing to impose that $\bar{T}_{\mathrm{s,pl}} = 0$, the perturbative problem has zero average temperature; hence, $T_{\infty} = T_{\mathrm{1D},\infty}$, simplifying the expression for spreading resistance. When a contact has a non-flat base, Eq. (8) must be used.

2 Previous Work

Contact resistance in single contacts is well documented in the literature. We note that rectangular and circular-cross section domains are referred to as flux channels and flux tubes, respectively. Cooper *et al.* [5] solved the canonical problem for the spreading resistance in a semi-infinite flux tube with a circular isothermal source surrounded by an adiabatic annulus along its base. A heat flux distribution resulting in an almost isothermal source was used to avoid a mixed boundary condition along the base of the domain. The heat flux is discontinuous along the circle separating the source from the adiabatic annulus. The results are accurate to within 2% for ratios of contact spot radius to cylinder radius up to 0.4, but then becomes inaccurate. Mikic [1] supported and expanded on the results from [5], developing results for contact resistance in flux tubes with constant heat flux at the source, as well as solving for contact resistance in flux channels with various contact spot boundary conditions. Negus and Yovanovich [7] used a superposition of flux distributions to extend the results of [5] to higher ratios of contact radius to cylinder radius. Hunter and Williams [8] discretized the integral equations developed by Sneddon [9] to compute spreading resistance in a flux tube for a true isothermal contact, solving for the so-called constriction alleviation factor (also called the constriction resistance parameter) from which spreading resistance follows. The analyses of these authors and the vast majority of subsequent ones assume a flat plane of contact. This is in contrast to the topography of real surfaces, in which micro-scale roughness is relevant.

Modeling of contact resistance sometimes considers micro-roughness indirectly as values of the average height and slope of the asperities on contacting surfaces are used to define a relationship between the distribution and size of contacts and other factors such as the load pressure and material hardness as per models by Cooper *et al.* [5] and Greenwood and Williamson [10]. The height and slope values can be captured through surface topography measurement techniques, such as profilometry, or estimated from the mean square roughness values typical of a manufacturing technique. The distributions are then coupled with spreading resistance expressions from models of single contacts with a flat plane of contact as discussed above. Combined they provide a model for contact resistance on the macro-scale. We develop spreading resistance expressions for non-flat contacts that better mimic the topology of real surfaces, and thus, when integrated into existing models, provide a better estimation of contact resistance.

Rather than focusing on the non-flatness of contacts, recent work has mainly focused on solving for spreading resistance assuming a flat plane of contact with increasing complexity; e.g., computing spreading resistance through stacks of thin materials as is often encountered in microelectronics packaging. This is made clear by comprehensive reviews of spreading and contact resistance by Yovanovich [11] in 2005 and later Razavi *et al.* [12] in 2016. Notably, however, some authors have examined the effect of non-flatness on single contacts. Madhusudana [13] used finite-difference simulations to quantify spreading resistance in conically-capped flux tubes. A flat, circular, isothermal source was placed at the truncated tip of a conical cap

Downloaded From: https://heattransfer.asmedigitalcollection.asme.org on 01/28/2019 Terms of Use: http://www.asme.org/about-asme/terms-of-use

Journal of Heat Transfer. Received July 24, 2018;
Accepted manuscript posted January 08, 2019. doi:10.1115/1.4042441
Copyright (c) 2019 by ASME

on a semi-infinite flux tube. They considered two cases: one in which the gap created by this conical cap was adiabatic and another in which it was filled with a fluid of low thermal conductivity. Sano [14] analytically studied the effect of non-flatness on electrical contact resistance for a single contact by modeling the shape of the contact as a hyperboloid of one sheet. This enabled them to solve for spreading resistance in a non-flat halfspace. Das and Sadhal [6] considered the Cartesian-geometry problem for flat contacts between semi-infinite materials of different thermal conductivities adjacent to sparsely distributed, circular-arc geometry gaps (not assumed to be of equal protrusion angle) filled with a third material of finite thermal conductivity. Bipolar coordinates were used and further details are provided by Das [15]. Das and Sadhal [16] then used their solution to the single-gap problem as a basis for the (symmetric) multi-gap one to capture higher-order interactions between gaps. To preserve analytical tractability, it was further assumed that the gaps were thin, which simplified the temperature distribution in them and their interaction. The temperature field was computed to $O[(1-\gamma)^6]$, where γ is the contact fraction, from which the contact resistance follows, although the closed-form expression is not provided due to its length.

Notably, this paper was inspired, in part, by work done to calculate apparent thermal and hydrodynamic slip lengths for flows over (biomimetic) superhydrophobic surfaces. When both problems are made dimensionless, solving for the apparent hydrodynamic slip length in linear-shear flows in the Cassie state over parallel ridge-type superhydrophobic surfaces is identical to solving for thermal spreading, and thus contact, resistance in Cartesian coordinates with an isothermal contact spot [17]. Indeed, solving for one immediately provides the result for the other; as such, one is able to pull liberally from the robust literature on apparent slip lengths. In Cartesian problems, contact resistance for the full range of geometric parameters is provided by Hodes *et al.* [4] for mating rough surfaces. The methodology and setup of the perturbation analysis in this paper is outlined by Sbragaglia and Prosperetti [18] and Lam *et al.* [19] in their work on apparent hydrodynamic and thermal slip, respectively, along superhydrophobic surfaces. Unlike those authors, however, we use reciprocity arguments based on Green's second integral identity following a perturbative approach introduced by Crowdy [20], also in the context of apparent hydrodynamic slip on superhydrophobic surfaces.

We capture the effect of the non-flat nature of real contacts on spreading resistance in a flux tube, where the analog with superhydrophobic surfaces no longer holds. We use a boundary perturbation of the solution of Hunter and Williams [8] to model the annulus outside of the contact spot as an adiabatic-arc, rather than a flat surface. In using this technique, we find contact resistance to the first order in $\tilde{\epsilon}$, where $\tilde{\epsilon}$ is one half the dimensionless curvature of the arc, and, importantly, without the need to fully resolve the correction to the temperature field due to boundary deflection. We quantify the increase in dimensionless contact resistance due to the curvature of the boundaries for the full range of contact angle (defined below) and constriction ratio (the ratio of contact spot radius to the radius of the entire cylinder) by using a numerical method for sufficiently large boundary deflection. Finally, when contact angle is negative we provide the decrease in spreading resistance.

3 Problem Formulation and Analysis

Figure 3 illustrates the axisymmetric nature of the flat and non-flat contacts under consideration. We require the formulation of two problems, i.e., the temperature field of a flat contact T_0 as shown in Fig. 4a) and that of a non-flat contact T. We exclusively consider a circular, isothermal region along the center of the base of the domain surrounded by an adiabatic annulus in a plan form view. When the annulus is flat we refer to the problem as the flat-contact problem and when it is not flat we refer to it as the non-flat contact problem. As the shape of the surface asperities is often unknown, the geometry of the nominal plane of contact is somewhat arbitrary. For example, the adiabatic region outside the contact area could be

Accepted Manuscript Not Copyedited

Downloaded From: https://heattransfer.asmedigitalcollection.asme.org on 01/28/2019 Terms of Use: http://www.asme.org/about-asme/terms-of-use

Journal of Heat Transfer. Received July 24, 2018;
Accepted manuscript posted January 08, 2019. doi:10.1115/1.4042441
Copyright (c) 2019 by ASME

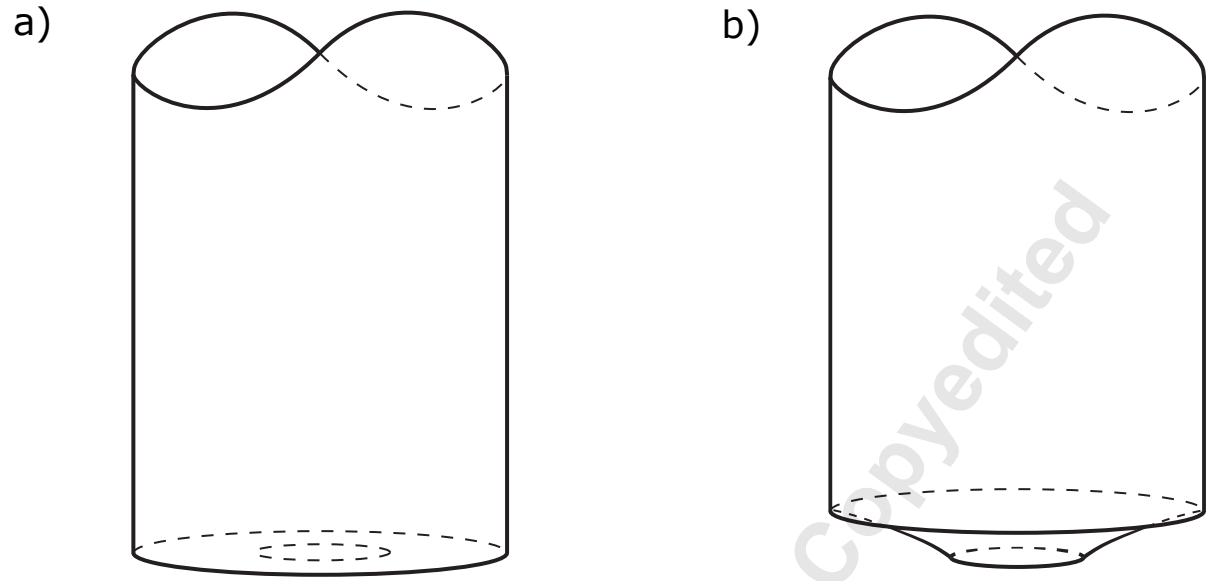


Figure 3: Schematics of the flat-contact modeling geometry a) and non-flat-contact modeling geometry b) . The contact spot is the circular section on the base.

modeled as concave, as in Fig. 4b), convex, as in Fig. 4c), or a straight line as in the numerical study by Madhusudana [13] and in Fig. 4d). We define T as the solution to the boundary value problem depicted in Fig. 4b); however, the methodology presented can also be used to solve for contact resistance of the geometry in Fig. 4c), which may be more physically realistic. This is discussed briefly in the Section 3.1. Again, we only need to consider the spreading resistance problems shown in Fig. 4, from which contact resistance for a symmetric contact follows [6]. We define c as the contact radius, b as the cylinder radius and $\phi = c/b$ as the constriction ratio. The contact angle α, is that between the tangent of the adiabatic-arc where it intersects the contact and the horizontal. It can be set equal to the average asperity slope of a surface. A positive contact angle corresponds to the arc penetrating into the solid, the relevant geometry for contact resistance.

For problems T_0 and T heat conduction is governed by the Laplace equation in axisymmetric, cylindrical coordinates as per

$$\nabla^2 T_0 = \nabla^2 T = 0 \tag{9}$$

There is no singularity at $r = 0$, and an adiabatic boundary condition exists along the outside radius of the cylinder such that

$$\frac{\partial T_0}{\partial r} = \frac{\partial T}{\partial r} = 0 \quad \text{for} \quad r = 0, \quad z \geq 0 \tag{10}$$

and

$$\frac{\partial T_0}{\partial r} = \frac{\partial T}{\partial r} = 0 \quad \text{for} \quad r = b, \quad z \geq 0 \tag{11}$$

A constant heat flux leaves the domain as $z \to \infty$ as per

$$\frac{\partial T_0}{\partial z} = \frac{\partial T}{\partial z} = -\frac{\bar{q}''}{k} \quad \text{for} \quad 0 \leq r \leq b, \quad z \to \infty \tag{12}$$

Accepted Manuscript Not Copyedited

Downloaded From: https://heattransfer.asmedigitalcollection.asme.org on 01/28/2019 Terms of Use: http://www.asme.org/about-asme/terms-of-use

Journal of Heat Transfer. Received July 24, 2018;
Accepted manuscript posted January 08, 2019. doi:10.1115/1.4042441
Copyright (c) 2019 by ASME

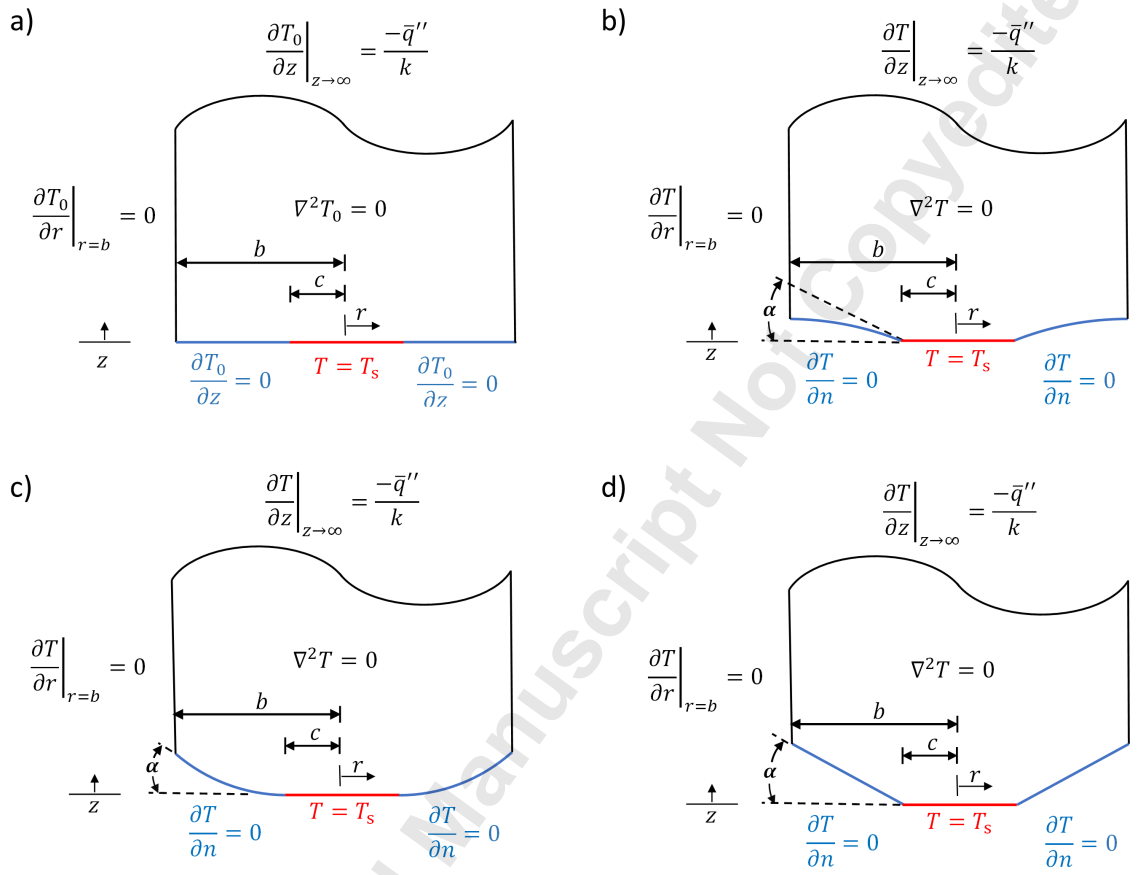


Figure 4: a) Dimensional flat-contact problem. b) Dimensional non-flat-contact problem with concave adiabatic-arc. c) Dimensional non-flat-contact problem with convex adiabatic-arc. d) Dimensional non-flat-contact problem with adiabatic-line. All problems are axisymmetric.

Accepted Manuscript Not Copyedited

Downloaded From: https://heattransfer.asmedigitalcollection.asme.org on 01/28/2019 Terms of Use: http://www.asme.org/about-asme/terms-of-use

Journal of Heat Transfer. Received July 24, 2018;
Accepted manuscript posted January 08, 2019. doi:10.1115/1.4042441
Copyright (c) 2019 by ASME

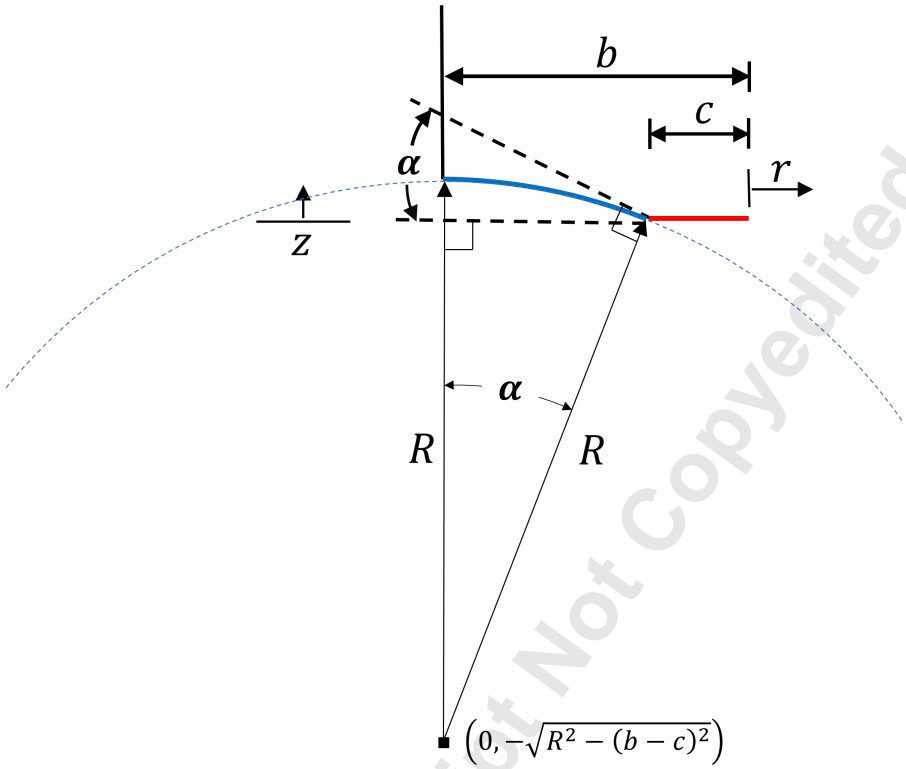


Figure 5: Depiction of the adiabatic circular-arc at the lower left-hand side of Fig. 4b).

We prescribe an isothermal boundary condition at the contact spot such that

$$T_0 = T = T_s \quad \text{for} \quad 0 \leq r < c, \quad z = 0 \tag{13}$$

The adiabatic condition along the area flanking the contact spot is

$$\begin{aligned} \frac{\partial T_0}{\partial z} &= 0 \quad \text{for} \quad c < r < b \\ \mathbf{n} \cdot \nabla T &= 0 \quad \text{for} \quad c < r < b \end{aligned} \tag{14}$$

where $\mathbf{n}$ is the vector normal to the adiabatic arc.

The z-coordinate along the adiabatic arc in Fig. 4b) is

$$z = \pm \left(\sqrt{R^2 - (r-b)^2} - \sqrt{R^2 - (b-c)^2} \right) \tag{15}$$

and depicted in Fig. 5. Taylor expanding the square roots yields

Accepted Manuscript Not Copyedited

Downloaded From: https://heattransfer.asmedigitalcollection.asme.org on 01/28/2019 Terms of Use: http://www.asme.org/about-asme/terms-of-use

Journal of Heat Transfer. Received July 24, 2018;
Accepted manuscript posted January 08, 2019. doi:10.1115/1.4042441
Copyright (c) 2019 by ASME

$$z = \pm \left\{ R \left[1 - \frac{1}{2} \left(\frac{r-b}{R} \right)^2 \right] - R \left[1 - \frac{1}{2} \left(\frac{b-c}{R} \right)^2 \right] \right\} + O\left(\frac{b^3}{R^3} \right) \tag{16}$$

The $(+)$ sign corresponds to the arc protruding upwards as in Fig. 6a), while the $(-)$ sign corresponds to it protruding downwards as in Fig. 6b) and is relevant to spreading, but not contact resistance as the abutting cylinders cannot overlap. We non-dimensionalize lengths by b and we place a tilde over our dimensionless quantities. The shape of the arc becomes

$$\tilde{z} = -\tilde{\epsilon}\tilde{\eta}(\tilde{r}) + O\left(\tilde{\epsilon}^3\right) \tag{17}$$

where $\tilde{\epsilon}$ is a small parameter defined by

$$\tilde{\epsilon} = \pm \frac{1}{2\tilde{R}} \tag{18}$$

and $\tilde{\eta}(\tilde{r})$ is a shape function defined by

$$\tilde{\eta}(\tilde{r}) = (\tilde{r}-1)^2 - (1-\phi)^2 \tag{19}$$

where $\phi = c/b$ is the constriction ratio. Positive and negative $\tilde{\epsilon}$ correspond to the arc protruding upward and downward and as per Figs. 6a) and 6b), respectively. Recall that the fraction of the projecting area of mating surfaces in contact is typically 1%-2%. This corresponds to approximately $0.1 < \phi < 0.15$; therefore, even for an unrealistically high contact angle with magnitude 90 degrees, $\tilde{\epsilon}$ is, at most, approximately 0.6 [2]. The cases of $\alpha = \pm 90^\circ$ are illustrated in Figs. 6c) and 6d), respectively, to highlight the range of angles considered in our study, but are only of theoretical interest. We note that $\tilde{\epsilon}$ represents one half of the dimensionless curvature of the arc, and from geometrical considerations

$$\tilde{\epsilon} = \frac{\sin(\alpha)}{2(1-\phi)} \tag{20}$$

It is important to note that the subsequent analysis is valid for any arc shape in which one half the dimensionless arc curvature is the small parameter and can be separated from a shape function. For example, in the case of a convex arc as depicted in Fig. 4c) a circle with radius R centered at $r = c$ and $z = R$ takes the form $z = \pm \left(-\sqrt{R^2 - (r-c)^2} + R \right)$, where the $(+)$ and $(-)$ refer to positive and negative values of α, respectively. Performing a binomial expansion of the square root yields

$$z = \pm \left(-R \left[1 - \frac{1}{2} \left(\frac{r-c}{R} \right)^2 \right] + R \right) + O\left(\frac{b^3}{R^3} \right) \tag{21}$$

We again nondimensionalize length by b and we place a tilde over our dimensionless quantities such that

$$\tilde{z} = -\tilde{\epsilon}\tilde{\eta}_{\text{convex}} + O\left(\tilde{\epsilon}^3\right) \tag{22}$$

where $\tilde{\epsilon}$ is the same as above and

$$\tilde{\eta}_{\text{convex}} = -(\tilde{r} - \phi)^2 \tag{23}$$

To calculate spreading resistance with the convex arc geometry one only needs to replace $\tilde{\eta}$ with $\tilde{\eta}_{\text{convex}}$ and proceed with the analysis below.

Accepted Manuscript Not Copyedited

Downloaded From: https://heattransfer.asmedigitalcollection.asme.org on 01/28/2019 Terms of Use: http://www.asme.org/about-asme/terms-of-use

Journal of Heat Transfer. Received July 24, 2018;
Accepted manuscript posted January 08, 2019. doi:10.1115/1.4042441
Copyright (c) 2019 by ASME

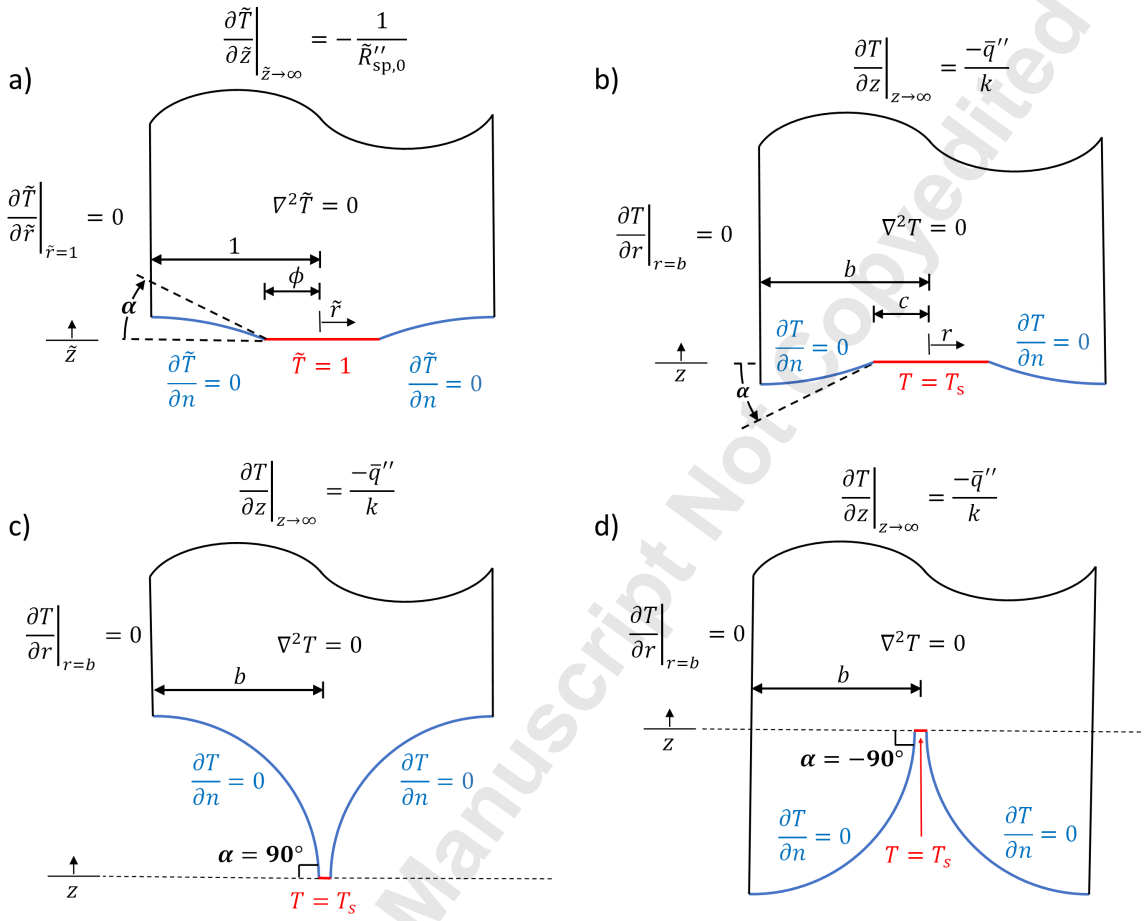


Figure 6: a) Upward-protruding adiabatic arc corresponding to positive ϵ with $c/b = 0.3$ and $\alpha = 25°$. b) Downward-protruding adiabatic arc corresponding to negative ϵ with $c/b = 0.3$ and $\alpha = -25°$. c) Upward-protruding adiabatic arc with $c/b = 0.05$ and $\alpha = 90°$. d) Downward-protruding adiabatic arc with $c/b = 0.05$ and $\alpha = -90°$.

Accepted Manuscript Not Copyedited

Downloaded From: https://heattransfer.asmedigitalcollection.asme.org on 01/28/2019 Terms of Use: http://www.asme.org/about-asme/terms-of-use

Journal of Heat Transfer. Received July 24, 2018;
Accepted manuscript posted January 08, 2019. doi:10.1115/1.4042441
Copyright (c) 2019 by ASME

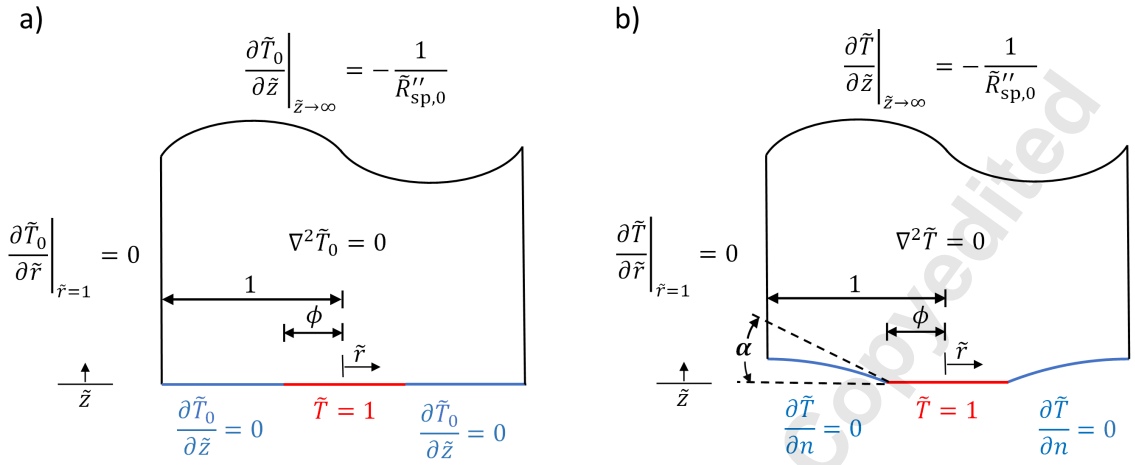


Figure 7: a) Dimensionless flat-contact problem. b) Dimensionless non-flat-contact problem.

We define the dimensionless temperature fields as

$$\tilde{T}_0 = \frac{T_0}{T_\mathrm{s}}, \qquad \tilde{T} = \frac{T}{T_\mathrm{s}} \tag{24}$$

which results in a unit temperature source. The dimensionless problems for the flat and non-flat contacts are shown in Figs. 7a) and 7b), respectively. To solve for spreading resistance in the flat contact problem we calculate the dimensionless heat flux through a semi-infinite cylinder with a specified temperature drop due to constriction or spreading ($\Delta\tilde{T}_{0,\mathrm{sp}} = \tilde{T}_{0,\mathrm{s}} - \tilde{T}_{0,\mathrm{s,pl}}$). Then, we assign this calculated heat flux to the non-flat contact problem to solve for the dimensionless temperature drop due to the combined effects of constriction or spreading and non-flatness, i.e., $\Delta\tilde{T}_{\mathrm{sp}} = (\tilde{T}_\mathrm{s} - \tilde{T}_{1\mathrm{D,s}}) - (\tilde{T}_\infty - \tilde{T}_{1\mathrm{D},\infty})$.

We summarize the solution of Hunter and Williams [8] which provides the dimensionless temperature field and dimensionless contact resistance of a flat contact. The governing equation is Laplace's Equation in axisymmetric $(\tilde{r}, \tilde{z})$ cylindrical coordinates. It follows from Eq. (8) and our subsequent prescription of a mean temperature of zero along $z = 0$ that in the dimensional problem $\Delta T_{0,\mathrm{sp}} = T_\mathrm{s}$, implying $R''_{\mathrm{sp}} = T_\mathrm{s}/\bar{q}''$. Then, defining non-dimensional spreading resistance as $\tilde{R}''_{\mathrm{sp}} = R''_{\mathrm{sp}} k/b$, the boundary conditions on Laplace's equation in the dimensionless problem become

$$\tilde{z} = 0 \quad \begin{cases} \tilde{T}_0 = 1 & 0 \le r < \phi \\ \frac{\partial \tilde{T}_0}{\partial \tilde{z}} = 0 & \phi < r \le 1 \end{cases} \tag{25}$$

$$\frac{\partial \tilde{T}_0}{\partial \tilde{z}} = -\frac{1}{\tilde{R}''_{\mathrm{sp}}} \quad \tilde{z} \to \infty \tag{26}$$

Accepted Manuscript Not Copyedited

Downloaded From: https://heattransfer.asmedigitalcollection.asme.org on 01/28/2019 Terms of Use: http://www.asme.org/about-asme/terms-of-use

Journal of Heat Transfer. Received July 24, 2018;
Accepted manuscript posted January 08, 2019. doi:10.1115/1.4042441
Copyright (c) 2019 by ASME

$$\frac{\partial \tilde{T}_0}{\partial \tilde{r}} = 0 \quad \tilde{r} = 0, 1 \tag{27}$$

where $\tilde{R}''_{\rm sp}$ is unknown.

Using separation of variables, the series solution which satisfies the homogeneous boundary conditions on $\tilde{r} = 0, 1$ and the inhomogeneous one as $\tilde{z} \to \infty$ is

$$\tilde{T}_0(\tilde{r}, \tilde{z}) = -\frac{1}{\tilde{R}''_{\rm sp,0}}\tilde{z} + \sum_{n=1}^{\infty} \lambda_n^{-1} C_n J_0(\lambda_n \tilde{r}) \exp(-\lambda_n \tilde{z}) \tag{28}$$

where J_0 is a Bessel function of the first kind of zeroth order and C_n are unknown coefficients. The eigenvalues λ_n satisfy $J_1(\lambda_n) = 0$. Applying Eq. (25) yields dual-series equations for C_n as

$$1 = \sum_{n=1}^{\infty} \lambda_n^{-1} C_n J_0(\lambda_n \tilde{r}) \quad \text{for} \quad 0 \le \tilde{r} < \phi \tag{29}$$

$$0 = -\frac{1}{\tilde{R}''_{\rm sp,0}} - \sum_{n=1}^{\infty} C_n J_0(\lambda_n \tilde{r}) \quad \text{for} \quad \phi < \tilde{r} \le 1 \tag{30}$$

Sneddon [9] provides a semi-analytical means to solve a more general form of these dual-series equations. It follows from his result that

$$\tilde{R}''_{\rm sp,0} = -\frac{1}{2\int_0^{\phi} h(t)\mathrm{d}t} \tag{31}$$

$$C_n = \frac{2}{J_0^2(\lambda_n)} \int_0^{\phi} h(t)\cos(t\lambda_n)\mathrm{d}t \tag{32}$$

where $h(t)$ is defined as the solution to the integral equation

$$h(t) - \int_0^{\phi} h(u) G_1(t, u)\mathrm{d}u = \frac{2}{\pi} \tag{33}$$

where

$$G_1(t, u) = \frac{4}{\pi} + \frac{4}{\pi^2} \int_0^{\infty} \frac{K_1(y)}{y I_1(y)} [2I_1(y) - y\cosh(uy)\cosh(ty)]\mathrm{d}y \tag{34}$$

and I_1 and K_1 are first-order modified Bessel functions of the first and second kind, respectively. We discretize and evaluate the integrals numerically using quadrature. We invert the resulting matrix to determine discrete values of $h(t)$ from which $\tilde{R}''_{\rm sp,0}$ and C_n are computed via Eqs. (31) and (32). We note that solving for spreading resistance in the flat-contact problem does not require the evaluation of C_n; however, these coefficients are needed for the non-flat-contact one.

Turning to the non-flat contact problem (see Fig. 4b)) and expressing the dimensionless temperature field for it as an expansion in $\tilde{\epsilon} \ll 1$, it takes the form

$$\tilde{T}(\tilde{r}, \tilde{z}) = \tilde{T}_0 + \tilde{\epsilon}\tilde{T}_1 + O(\tilde{\epsilon}^2) \tag{35}$$

Accepted Manuscript Not Copyedited

Downloaded From: https://heattransfer.asmedigitalcollection.asme.org on 01/28/2019 Terms of Use: http://www.asme.org/about-asme/terms-of-use

Journal of Heat Transfer. Received July 24, 2018;
Accepted manuscript posted January 08, 2019. doi:10.1115/1.4042441
Copyright (c) 2019 by ASME

where $\tilde{\epsilon}\tilde{T}_1$ is the change in $\tilde{T}$ to the first order in $\tilde{\epsilon}$ that results from the deflection of the boundary. Hence,

$$\tilde{T} = -\frac{1}{\tilde{R}''_{\mathrm{sp},0}}\tilde{z} + \sum_{n=1}^{\infty} \lambda_n^{-1} C_n J_0(\lambda_n \tilde{r}) \exp(-\lambda_n \tilde{z}) + \tilde{\epsilon}\tilde{T}_1 + O(\tilde{\epsilon}^2) \tag{36}$$

Since the far-field boundary condition on $\tilde{T}$ is constant heat flux, as $\tilde{z} \to \infty$, $\tilde{\epsilon}\tilde{T}_1$ must converge to a constant, denoted as $\Delta\tilde{T}_{\mathrm{p}}$, such that as $\tilde{z} \to \infty$, $\tilde{T}_\infty \to \tilde{T}_{1\mathrm{D},\infty} + \Delta\tilde{T}_{\mathrm{p}}$. For a not-flat contact with $\tilde{T}_{\mathrm{s}} = 1$, the temperature change due to spreading or constriction is given by $\Delta\tilde{T}_{\mathrm{sp}} = (1 - \tilde{T}_{1\mathrm{D,s}}) - (\tilde{T}_\infty - \tilde{T}_{1\mathrm{D},\infty})$, evaluated in this case as $\Delta\tilde{T}_{\mathrm{sp}} = 1 - \Delta\tilde{T}_{\mathrm{p}}$.

It is convenient in the application of Green's second identity for the source temperature in both problems to be zero. Hence, we introduce dimensionless temperature fields $\tilde{T}'_0 = \tilde{T}_0 - 1$ and $\tilde{T}' = \tilde{T} - \tilde{T}_{\mathrm{s}}$, where $\tilde{T}'_0$ and $\tilde{T}'$ represent the flat contact and non-flat problems with zero source temperature, respectively, as per

$$\tilde{T}'_0 = -\frac{1}{\tilde{R}''_{\mathrm{sp},0}}\tilde{z} + \sum_{n=1}^{\infty} \lambda_n^{-1} C_n J_0(\lambda_n \tilde{r}) \exp(-\lambda_n \tilde{z}) - 1 \tag{37}$$

$$\tilde{T}' = -\frac{1}{\tilde{R}''_{\mathrm{sp},0}}\tilde{z} + \sum_{n=1}^{\infty} \lambda_n^{-1} C_n J_0(\lambda_n \tilde{r}) \exp(-\lambda_n \tilde{z}) - 1 + \tilde{\epsilon}\tilde{T}_1 + O(\tilde{\epsilon}^2) \tag{38}$$

as shown in Fig. 8. Then, in the limit as $\tilde{z} \to \infty$,

$$\tilde{T}'_0 = -\frac{1}{\tilde{R}''_{\mathrm{sp},0}}\tilde{z} - 1 \tag{39}$$

$$\tilde{T}' = -\frac{1}{\tilde{R}''_{\mathrm{sp},0}}\tilde{z} - \Delta\tilde{T}_{\mathrm{sp}} + O(\tilde{\epsilon}^2) \tag{40}$$

The following steps emulate the approach of Crowdy [20] for a mathematically similar problem. Green's second identity on the domain D of the non-flat contact states that

$$\iiint_D \left(\tilde{T}' \nabla^2 \tilde{T}'_0 - \tilde{T}'_0 \nabla^2 \tilde{T}'\right) \mathrm{d}V = \oiint_{\partial D} \left(\tilde{T}' \frac{\partial \tilde{T}'_0}{\partial n} - \tilde{T}'_0 \frac{\partial \tilde{T}'}{\partial n}\right) \mathrm{d}A \tag{41}$$

where n is the direction of the outward pointing unit normal. The volume integral disappears as both fields are governed by Laplace's Equation. Using the adiabatic boundary condition at $\tilde{r} = 1$, zero temperature boundary condition at the source and adiabatic boundary condition along the arc and noting that the derivatives for the prime functions are the same as those of the original ones, Eq. (41) simplifies to

$$0 = \iint_{\tilde{z}\to\infty} \tilde{T}' \frac{\partial \tilde{T}_0}{\partial n} - \tilde{T}'_0 \frac{\partial \tilde{T}}{\partial n} \mathrm{d}A + \iint_{\tilde{z}=-\tilde{\epsilon}\tilde{\eta}} \tilde{T}' \frac{\partial \tilde{T}_0}{\partial n} \mathrm{d}A \tag{42}$$

Evaluating the far-field integral yields

$$0 = \left[\left(\frac{1}{\tilde{R}''_{\mathrm{sp},0}}\tilde{z} + \Delta\tilde{T}_{\mathrm{sp}}\right) - \left(\frac{1}{\tilde{R}''_{\mathrm{sp},0}}\tilde{z} + 1\right)\right] \frac{\pi}{\tilde{R}''_{\mathrm{sp},0}} + \int_\phi^1 \left[\left(\tilde{T}'(\tilde{r}, -\tilde{\epsilon}\tilde{\eta}) \frac{\partial \tilde{T}_0(\tilde{r}, -\tilde{\epsilon}\tilde{\eta})}{\partial n}\right) \sqrt{1 - \left(\tilde{\epsilon}\frac{\mathrm{d}\tilde{\eta}}{\mathrm{d}\tilde{r}}\right)^2}\, 2\pi\tilde{r}\mathrm{d}\tilde{r}\right] + O(\tilde{\epsilon}^2) \tag{43}$$

Plugging in for $\tilde{T}'$ and rearranging results in

Accepted Manuscript Not Copyedited

Downloaded From: https://heattransfer.asmedigitalcollection.asme.org on 01/28/2019 Terms of Use: http://www.asme.org/about-asme/terms-of-use

Journal of Heat Transfer. Received July 24, 2018;
Accepted manuscript posted January 08, 2019. doi:10.1115/1.4042441
Copyright (c) 2019 by ASME

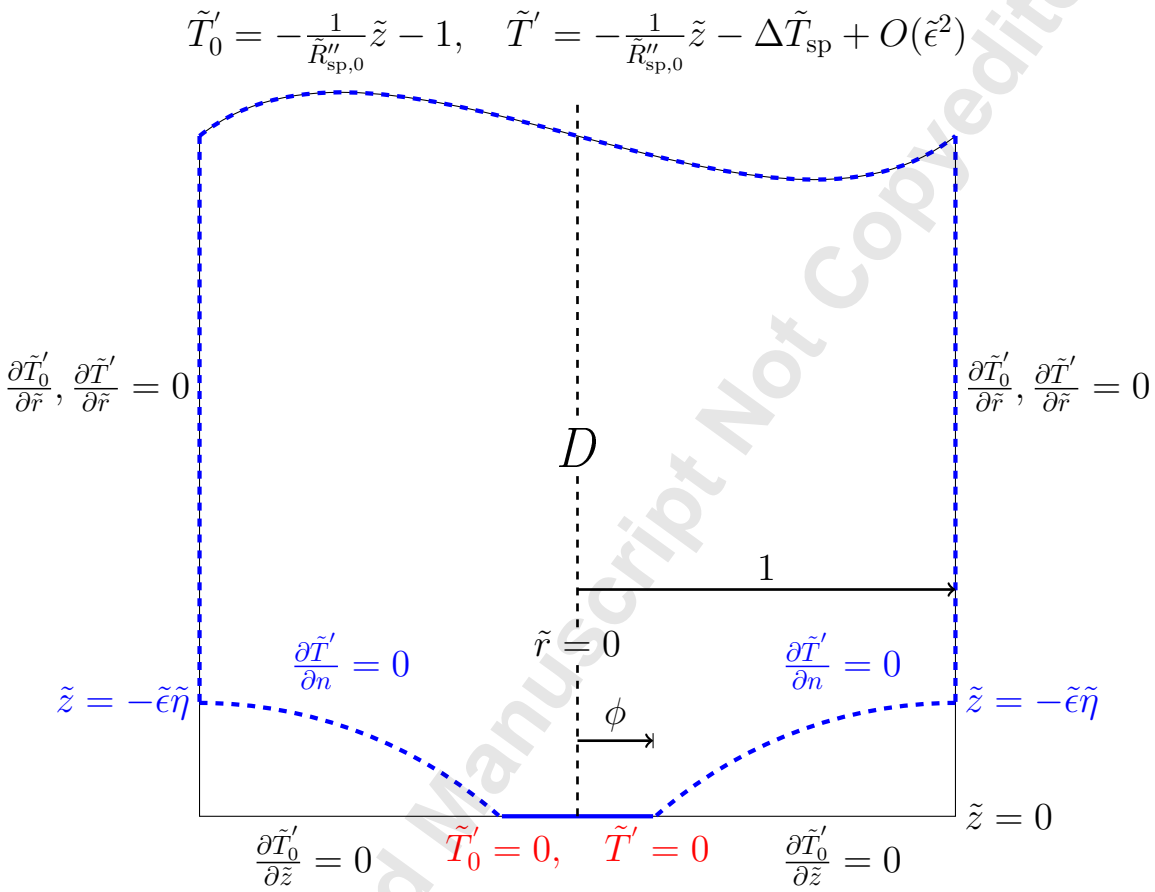


Figure 8: Domain D (dashed region) with all relevant boundary conditions

Accepted Manuscript Not Copyedited

Downloaded From: https://heattransfer.asmedigitalcollection.asme.org on 01/28/2019 Terms of Use: http://www.asme.org/about-asme/terms-of-use

Journal of Heat Transfer. Received July 24, 2018;
Accepted manuscript posted January 08, 2019. doi:10.1115/1.4042441
Copyright (c) 2019 by ASME

$$\Delta\tilde{T}_{\rm sp}-1=-2\pi\frac{\tilde{R}''_{\rm sp,0}}{\pi}\int_{\phi}^{1}\left[\left(\tilde{T}_0(\tilde{r},-\tilde{\epsilon}\tilde{\eta})+\tilde{\epsilon}\tilde{T}_1(\tilde{r},-\tilde{\epsilon}\tilde{\eta})-1\right)\frac{\partial\tilde{T}_0(\tilde{r},-\tilde{\epsilon}\tilde{\eta})}{\partial n}\right]\sqrt{1-\left(\tilde{\epsilon}\frac{{\rm d}\tilde{\eta}}{{\rm d}\tilde{r}}\right)^2}\,\tilde{r}{\rm d}\tilde{r}+O(\tilde{\epsilon}^2) \quad (44)$$

Taking the outward facing unit normal vector as $n=(1/|\mathbf{n}|)\left[-\tilde{\epsilon}({\rm d}\tilde{\eta}/{\rm d}\tilde{r})\hat{\mathbf{r}}-\hat{\mathbf{z}}\right]$,

$$\left.\frac{\partial\tilde{T}_0}{\partial n}\right|_{\tilde{z}=-\tilde{\epsilon}\tilde{\eta}}=-\frac{1}{|\mathbf{n}|}\left(\tilde{\epsilon}\frac{{\rm d}\tilde{\eta}}{{\rm d}\tilde{r}}\left.\frac{\partial\tilde{T}_0}{\partial\tilde{r}}\right|_{\tilde{z}=-\tilde{\epsilon}\tilde{\eta}}+\left.\frac{\partial\tilde{T}_0}{\partial\tilde{z}}\right|_{\tilde{z}=-\tilde{\epsilon}\tilde{\eta}}\right) \quad (45)$$

Taylor expansions of $\partial\tilde{T}_0/\partial\tilde{r}$ and $\partial\tilde{T}_0/\partial\tilde{z}$ about $\tilde{z}=0$ are

$$\left.\frac{\partial\tilde{T}_0}{\partial\tilde{r}}\right|_{\tilde{z}=-\tilde{\epsilon}\tilde{\eta}}=\left.\frac{\partial\tilde{T}_0}{\partial\tilde{r}}\right|_{\tilde{z}=0}+O(\tilde{\epsilon}) \quad (46)$$

$$\left.\frac{\partial\tilde{T}_0}{\partial\tilde{z}}\right|_{\tilde{z}=-\tilde{\epsilon}\tilde{\eta}}=\left.\frac{\partial\tilde{T}_0}{\partial\tilde{z}}\right|_{\tilde{z}=0}-\tilde{\epsilon}\tilde{\eta}\left.\frac{\partial^2\tilde{T}_0}{\partial\tilde{z}^2}\right|_{\tilde{z}=0}+O(\tilde{\epsilon}^2) \quad (47)$$

respectively. Substituting Eqs. (46), (47) and $|\mathbf{n}|=1+O(\tilde{\epsilon}^2)$ into Eq. (45), it becomes

$$\begin{aligned}\left.\frac{\partial\tilde{T}_0}{\partial\hat{n}}\right|_{\tilde{z}=-\tilde{\epsilon}\tilde{\eta}}=&-\left[\tilde{\epsilon}\frac{{\rm d}\tilde{\eta}}{{\rm d}\tilde{r}}\left(\left.\frac{\partial\tilde{T}_0}{\partial\tilde{r}}\right|_{\tilde{z}=0}+O(\tilde{\epsilon})\right)\right.\\&\left.+\left.\frac{\partial\tilde{T}_0}{\partial\tilde{z}}\right|_{\tilde{z}=0}-\tilde{\epsilon}\tilde{\eta}\left.\frac{\partial^2\tilde{T}_0}{\partial\tilde{z}^2}\right|_{\tilde{z}=0}+O(\tilde{\epsilon}^2)\right]\end{aligned} \quad (48)$$

However, since the integral is evaluated outside of the contact spot, $\left.\partial\tilde{T}_0/\partial\tilde{z}\right|_{\tilde{z}=0}=0$ and Eq. (48) becomes

$$\left.\frac{\partial\tilde{T}_0}{\partial n}\right|_{\tilde{z}=-\tilde{\epsilon}\tilde{\eta}}=-\tilde{\epsilon}\left(\frac{{\rm d}\tilde{\eta}}{{\rm d}\tilde{r}}\left.\frac{\partial\tilde{T}_0}{\partial\tilde{r}}\right|_{\tilde{z}=0}-\tilde{\eta}\left.\frac{\partial^2\tilde{T}_0}{\partial\tilde{z}^2}\right|_{\tilde{z}=0}\right)+O(\tilde{\epsilon}^2) \quad (49)$$

Also, Taylor expanding $\tilde{T}_0$ about $\tilde{z}=0$

$$\left.\tilde{T}_0\right|_{\tilde{z}=-\tilde{\epsilon}\tilde{\eta}}=\left.\tilde{T}_0\right|_{\tilde{z}=0}+O(\tilde{\epsilon}) \quad (50)$$

Then,

$$\left(\left.\tilde{T}_0\right|_{\tilde{z}=-\tilde{\epsilon}\tilde{\eta}}+\tilde{\epsilon}\left.\tilde{T}_1\right|_{\tilde{z}=-\tilde{\epsilon}\tilde{\eta}}\right)\left.\frac{\partial\tilde{T}_0}{\partial\hat{n}}\right|_{\tilde{z}=-\tilde{\epsilon}\tilde{\eta}}=-\tilde{\epsilon}\left.\tilde{T}_0\right|_{\tilde{z}=0}\left(\frac{{\rm d}\tilde{\eta}}{{\rm d}\tilde{r}}\left.\frac{\partial\tilde{T}_0}{\partial\tilde{r}}\right|_{\tilde{z}=0}-\tilde{\eta}\left.\frac{\partial^2\tilde{T}_0}{\partial\tilde{z}^2}\right|_{\tilde{z}=0}\right)+O(\tilde{\epsilon}^2) \quad (51)$$

i.e., we can ignore $\tilde{T}_1$ to the first-order in $\tilde{\epsilon}$. Using Eq. (51) and expanding the square root term on the left-hand side as per the binomial theorem gives

$$\int_{\phi}^{1}\left[\left(\tilde{T}_0+\tilde{\epsilon}\tilde{T}_1-1\right)\frac{\partial\tilde{T}_0}{\partial\hat{n}}\right]\sqrt{1-\left(\tilde{\epsilon}\frac{{\rm d}\tilde{n}}{{\rm d}\tilde{r}}\right)^2}\,2\pi\tilde{r}{\rm d}\tilde{r}=-2\pi\tilde{\epsilon}\int_{\phi}^{1}\tilde{r}\left(\left.\tilde{T}_0\right|_{\tilde{z}=0}-1\right)\left(\frac{{\rm d}\tilde{\eta}}{{\rm d}\tilde{r}}\left.\frac{\partial\tilde{T}_0}{\partial\tilde{r}}\right|_{\tilde{z}=0}-\tilde{\eta}\left.\frac{\partial^2\tilde{T}_0}{\partial\tilde{z}^2}\right|_{\tilde{z}=0}\right){\rm d}\tilde{r}+O(\tilde{\epsilon}^2) \quad (52)$$

Accepted Manuscript Not Copyedited

Downloaded From: https://heattransfer.asmedigitalcollection.asme.org on 01/28/2019 Terms of Use: http://www.asme.org/about-asme/terms-of-use

Journal of Heat Transfer. Received July 24, 2018;
Accepted manuscript posted January 08, 2019. doi:10.1115/1.4042441
Copyright (c) 2019 by ASME

Thus, substituting Eq. (52) into Eq. (44) gives

$$\Delta\tilde{T}_{\rm sp} - 1 = 2\tilde{\epsilon}\tilde{R}''_{\rm sp,0}\int_{\phi}^{1}\tilde{r}\left(\left.\tilde{T}_0\right|_{\tilde{z}=0} - 1\right)\left(\frac{{\rm d}\tilde{\eta}}{{\rm d}\tilde{r}}\left.\frac{\partial\tilde{T}_0}{\partial\tilde{r}}\right|_{\tilde{z}=0} - \tilde{\eta}\left.\frac{\partial^2\tilde{T}_0}{\partial\tilde{z}^2}\right|_{\tilde{z}=0}\right){\rm d}\tilde{r} + O(\tilde{\epsilon}^2) \tag{53}$$

It follows from our prescription of dimensionless heat flux as $1/\tilde{R}''_{\rm sp,0}$ that $\tilde{R}''_{\rm sp} = \Delta\tilde{T}_{\rm sp}\tilde{R}''_{\rm sp,0}$ and

$$\tilde{R}''_{\rm sp} = \tilde{R}''_{\rm sp,0} + 2\tilde{\epsilon}\left(\tilde{R}''_{\rm sp,0}\right)^2\int_{\phi}^{1}\tilde{r}\left(\left.\tilde{T}_0\right|_{\tilde{z}=0} - 1\right)\left(\frac{{\rm d}\tilde{\eta}}{{\rm d}\tilde{r}}\left.\frac{\partial\tilde{T}_0}{\partial\tilde{r}}\right|_{\tilde{z}=0} - \tilde{\eta}\left.\frac{\partial^2\tilde{T}_0}{\partial\tilde{z}^2}\right|_{\tilde{z}=0}\right){\rm d}\tilde{r} + O(\tilde{\epsilon}^2) \tag{54}$$

The integral can be evaluated, with $g(\phi)$ and $h(\phi)$ given in Appendix B of Mayer [21], yielding

$$\tilde{R}''_{\rm sp} = \tilde{R}''_{\rm sp,0} + 2\tilde{\epsilon}\left(\tilde{R}''_{\rm sp,0}\right)^2\left[g(\phi) - h(\phi)\right] \tag{55}$$

The dimensional spreading resistance is

$$R''_{\rm sp} = \frac{b}{k}\tilde{R}''_{\rm sp} \tag{56}$$

From this we can calculate an expression for $R''_{\rm tc}$ by adding two spreading resistance in series such that

$$R''_{\rm tc} = \frac{2b}{k_{12}}\tilde{R}''_{\rm sp} \tag{57}$$

where

$$\frac{1}{k_{12}} = \frac{1}{2}\left(\frac{1}{k_1} + \frac{1}{k_2}\right) \tag{58}$$

where k_1 and k_2 are the thermal conductivities of contacting materials 1 and 2, respectively. Often, this dimensional thermal contact resistance expression of a single contact is written as a heat transfer (contact conductance) coefficient h_c, i.e., $h_c = 1/R''_{\rm tc}$ [5].

4 Numerical Analysis

We validated our asymptotic model and extended it to arbitrary contact angle using the finite element method (FEA). The partial differential equation solver in MATLAB was used to compute the dimensionless temperature field in the solid, $\tilde{T}_{\rm n}$. It was compared to that with no adiabatic annulus, $\tilde{T}_{\rm 1D,}$, having the same height, width, and dimensionless heat flux through it, to find spreading resistance as per Eq. (8) such that

$$\tilde{R}''_{\rm sp,n} = \tilde{R}''_{\rm t,n} - \tilde{R}''_{\rm 1D,n} = \tilde{R}''_{\rm sp,0}\left[\left(\tilde{T}_{\rm n,s} - \tilde{T}_{\rm n,\infty}\right) - \left(\tilde{T}_{\rm 1D,s} - \tilde{T}_{\rm 1D,\infty}\right)\right] \tag{59}$$

The axisymmetric Laplace's equation was solved with relevant boundary condtions. $\tilde{T}_{\rm 1D,s}$ was set to 0 and $\tilde{T}_{\rm n,s}$ set equal to 1 on the isothermal contact spot. In solving for $\tilde{T}_{\rm n}$, an adiabatic arc was placed outside of the isothermal contact. The edges of the domain were specified as adiabatic and the heat flux at the far-field was specified as $-1/\tilde{R}''_{\rm sp,0}$. The height of the domain was 5 times the width of the domain as this was sufficient to ensure one dimensional flow at the far-field. A triangular mesh was adapted and refined multiple times to ensure mesh independence and until the difference in far-field temperature between subsequent iterations was less than 10^{-8}. This resulted in an average of around 800,000 elements in the domain. We captured the singularity at $(\phi, 0)$ as discussed later in Section 6.

Accepted Manuscript Not Copyedited

Downloaded From: https://heattransfer.asmedigitalcollection.asme.org on 01/28/2019 Terms of Use: http://www.asme.org/about-asme/terms-of-use

Journal of Heat Transfer. Received July 24, 2018;
Accepted manuscript posted January 08, 2019. doi:10.1115/1.4042441
Copyright (c) 2019 by ASME

5 Results

To solve the flat contact problem we truncated our infinite series at $N = 1500$. The N coefficients were solved by numerically evaluating the integrals given by Sneddon [9] to generate an $N \times N$ matrix that satisfied Eq. (33). We did this for 1000 evenly-spaced constriction ratios in $0 < \phi < 1$. Using these calculated coefficients, we then evaluated Eq. (54) for different contact angles in the same domain. Dimensionless spreading resistance against constriction ratio is plotted in Fig. 9 for a range of contact angles from $-30°$ to $30°$. It includes FEA numerical data. Recall that negative contact angles are not relevant to contact resistance as opposed to spreading resistance. In the limit as $\phi \to 0$, the spreading resistance asymptotes to resemble that of an adiabatic boundary at $\tilde{z} = 0$, i.e., infinity. Conversely, in the limit as $\phi \to 1$, it disappears. As the base of the contacting cylinders is perturbed from the flat baseline, the spreading resistance is noticeably affected. For arc protrusion into the cylinder, corresponding to $\alpha > 0°$, the total available volume for heat conduction is decreased, increasing spreading resistance. Conversely, for $\alpha < 0°$, the available volume for heat conduction is increased, decreasing spreading resistance.

As expected, the effect of non-flatness is most apparent for lower constriction ratios, showing, e.g., a 15% increase in spreading resistance when compared to the flat contact for $\alpha = 20°$ at $\phi = 0.01$. Since the increase in spreading resistance is most notable for small constriction ratio, spreading resistance in real contacts is greatly affected. The interval $0.1 \leq \phi \leq 0.2$ captures the range of constriction ratios that most contacts exhibit [7] and we see significant effects on spreading resistance in this range, even for small boundary deflection. For example, when $\alpha = 5°$ we see a rather modest increase in spreading resistance of approximately 3.5% for $\phi = 0.1$ and 3.4% for $\phi = 0.2$. However, when $\alpha = 20°$, we see a significant increase of approximately 13% for $\phi = 0.1$ and 11% for $\phi = 0.2$. This highlights the importance of including non-flatness in the modeling of single contacts when modeling contact resistance.

Additionally, we see good agreement with the numerical results from Madhusudana [13] in their analysis of conical-tipped cylindrical contacts with adiabatic gaps for small ϕ and α. For their geometry corresponding to a contact angle of $\alpha = 22.5°$, they report a dimensionless spreading resistance of around 8 for $\phi = 0.1$ and around 2.4 for $\phi = 0.25$ as per Fig. 3 in their paper. Our analytical method with $\alpha = 22.5°$ gives $\tilde{R}''_{\text{sp}} = 7.70$ for $\phi = 0.1$ and $\tilde{R}''_{\text{sp}} = 2.30$ for $\phi = 0.1$ as per Fig. 9, differences of 4.00% and 4.35% respectively. This agreement is expected at sufficiently small contact angle because the parabolic shape of our adiabatic-arc geometry closely resembles a straight line, as per Fig. 6a).

Table 1 compares dimensionless spreading resistance obtained in the perturbation method, $\tilde{R}''_{\text{sp}}$, to that numerically obtained, $\tilde{R}''_{\text{sp,N}}$. Percent error is calculated as $100\times[(\tilde{R}''_{\text{sp}} - \tilde{R}_{\text{sp,n}})/\tilde{R}''_{\text{sp}}]$ such that it is negative when our asymptotic model *underestimates* spreading resistance. Interestingly, the percent error calculated is always negative. For positive contact angle this is because the adiabatic-arc is circular in the numerical analysis, whereas in the asymptotic analysis it is approximated as parabolic. The domain volume is higher in the case of the parabolic boundary and thus spreading resistance is reduced. However, if this argument were used for negative contact angles, one would expect the analysis to overestimate spreading resistance, which is not the case. For negative contact angle, the underestimation of spreading resistance is due to the assumption in the analysis that the effect on spreading resistance of a boundary deflection has negative mirror symmetry about $\tilde{z} = 0$, i.e, $\tilde{\epsilon}|_{\alpha} = -\tilde{\epsilon}|_{-\alpha}$ for the same constriction ratio. However, this assumption incorrectly assumes that in the two cases heat flow is affected similarly. In the case of positive contact angle, the heat is forced through a narrowed domain. For negative contact angle, heat is not forced through the new domain in the same way. Rather, the boundary deflection creates a small volume addition with adiabatic edges for heat to pool. Therefore, one would expect *alleviation* of spreading resistance due to a negative contact angle to be less than the *increase* in spreading resistance due to a positive contact angle of the same magnitude. Hence, our assumption of mirror symmetry leads the analysis to underestimate spreading resistance for cases with

Downloaded From: https://heattransfer.asmedigitalcollection.asme.org on 01/28/2019 Terms of Use: http://www.asme.org/about-asme/terms-of-use

Journal of Heat Transfer. Received July 24, 2018;
Accepted manuscript posted January 08, 2019. doi:10.1115/1.4042441
Copyright (c) 2019 by ASME

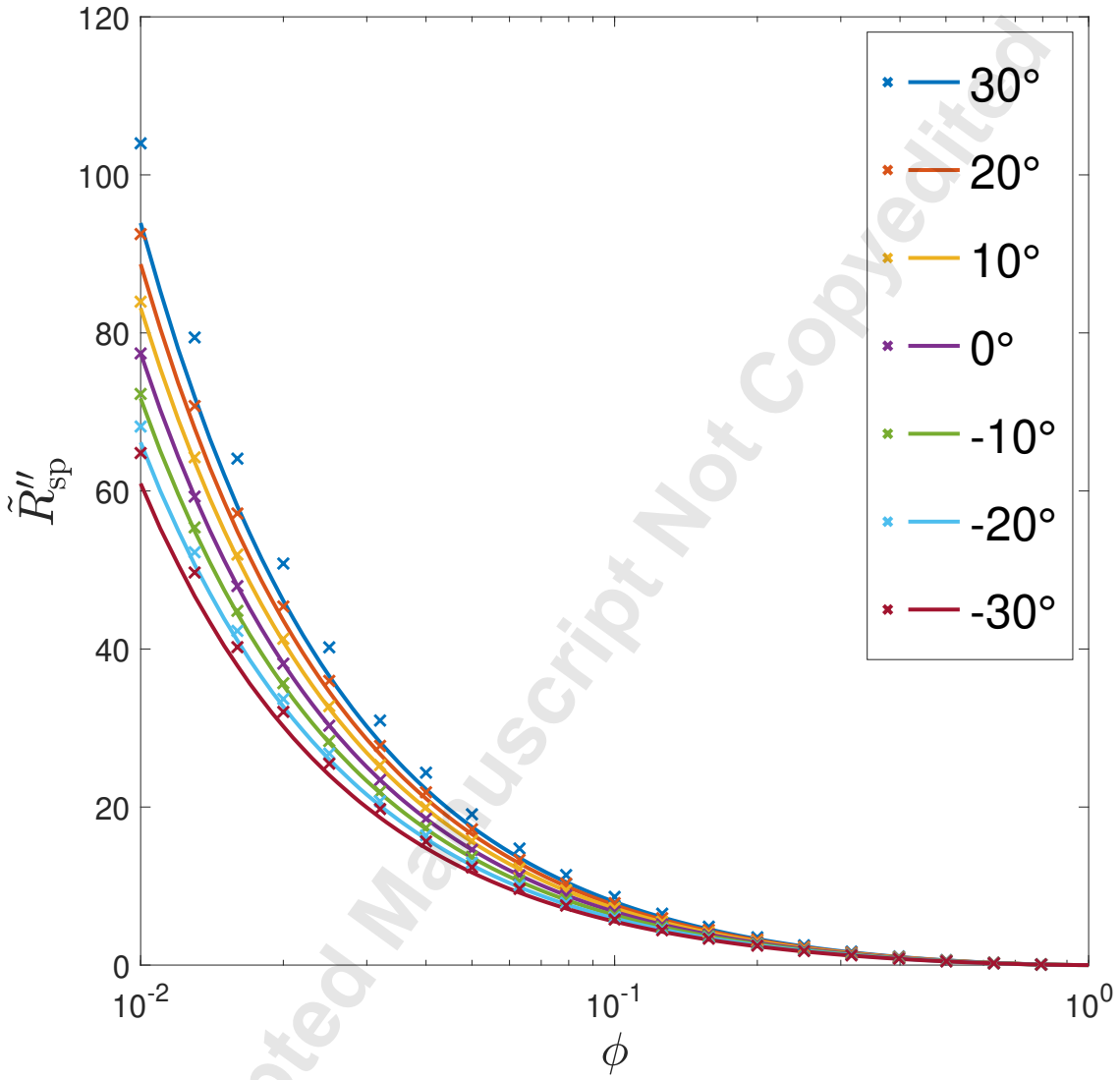


Figure 9: Dimensionless spreading resistance versus constriction ratio, ϕ, for selected contact angles, α.

Accepted Manuscript Not Copyedited

Downloaded From: https://heattransfer.asmedigitalcollection.asme.org on 01/28/2019 Terms of Use: http://www.asme.org/about-asme/terms-of-use

Journal of Heat Transfer. Received July 24, 2018;
Accepted manuscript posted January 08, 2019. doi:10.1115/1.4042441
Copyright (c) 2019 by ASME

ϕ	α	$\tilde{\epsilon}$	$\tilde{R}''_{\text{sp}}$	$\tilde{R}''_{\text{sp,n}}$	% Error
0.01	20	0.17	88.8	92.5	-4.21
0.01	15	0.13	86.0	87.9	-2.24
0.01	10	0.09	83.2	84.0	-0.93
0.01	5	0.04	80.3	80.5	-0.19
0.01	-5	-0.04	74.5	74.9	-0.49
0.01	-10	-0.09	71.7	72.6	-1.24
0.01	-15	-0.13	68.8	70.6	-2.53
0.01	-20	-0.17	66.1	68.7	-4.04
0.1	20	0.19	7.60	7.85	-3.26
0.1	15	0.14	7.39	7.52	-1.74
0.1	10	0.10	7.18	7.23	-0.73
0.1	5	0.05	6.97	6.98	-0.15
0.1	-5	-0.05	6.53	6.54	-0.16
0.1	-10	-0.10	6.32	6.36	-0.63
0.1	-15	-0.14	6.12	6.2	-1.35
0.1	-20	-0.19	5.90	6.04	-2.32
0.25	20	0.23	2.27	2.33	-2.53
0.25	15	0.17	2.22	2.25	-1.36
0.25	10	0.12	2.16	2.17	-0.56
0.25	5	0.06	2.11	2.11	-0.11
0.25	-5	-0.06	2.00	2.00	-0.11
0.25	-10	-0.12	1.94	1.95	-0.48
0.25	-15	-0.17	1.89	1.91	-1.04
0.25	-20	-0.23	1.83	1.86	-1.64

Table 1: Comparison of perturbaton method values of $\tilde{R}''_{\text{sp}}$ to numerical values of it, $\tilde{R}''_{\text{sp,n}}$.

negative contact angles as well.

As expected, we see excellent agreement with the analytical results for small $\tilde{\epsilon}$ and increasing divergence for larger values of it. Figure 10 compares dimensionless spreading resistance from our two models for $0.1 < \phi < 0.25$, a range that captures the typical range of constriction ratios for contact resistance problems [7] and shows good agreement between our asymptotic model and the FEA. After validating our model with numerical simulation for small $\tilde{\epsilon}$, we also used it to show when our analytical model diverges from the numerical model. Figure 9 depicts numerical, as well as analytical, results for contact angles between $-30°$ and $30°$. It is clear that the numerical model matches our model fairly well for $\alpha < 20°$, but at $\alpha = 30°$ it exhibits around a 10% error.

Numerical results for the spreading resistance results include the full $-90°$ and $90°$ contact angle range, completing the parameter space. Figure 11 depicts dimensionless spreading resistance for all contact angles $\geq 0°$, revealing a very large increase in thermal resistance at high contact angles. Indeed, as $\alpha \to 90°$, the cross section of the adiabatic-arc becomes a quarter circle centered at $(1, 0)$ with radius of $1 - \phi$ as depicted in Fig. 6c). Thus the adiabatic surface formed by this perturbed arc constricts heat flow for much greater distances from the source plane than for lesser contact angles. This too explains large asymptotic growth in

Accepted Manuscript Not Copyedited

Downloaded From: https://heattransfer.asmedigitalcollection.asme.org on 01/28/2019 Terms of Use: http://www.asme.org/about-asme/terms-of-use

Journal of Heat Transfer. Received July 24, 2018;
Accepted manuscript posted January 08, 2019. doi:10.1115/1.4042441
Copyright (c) 2019 by ASME

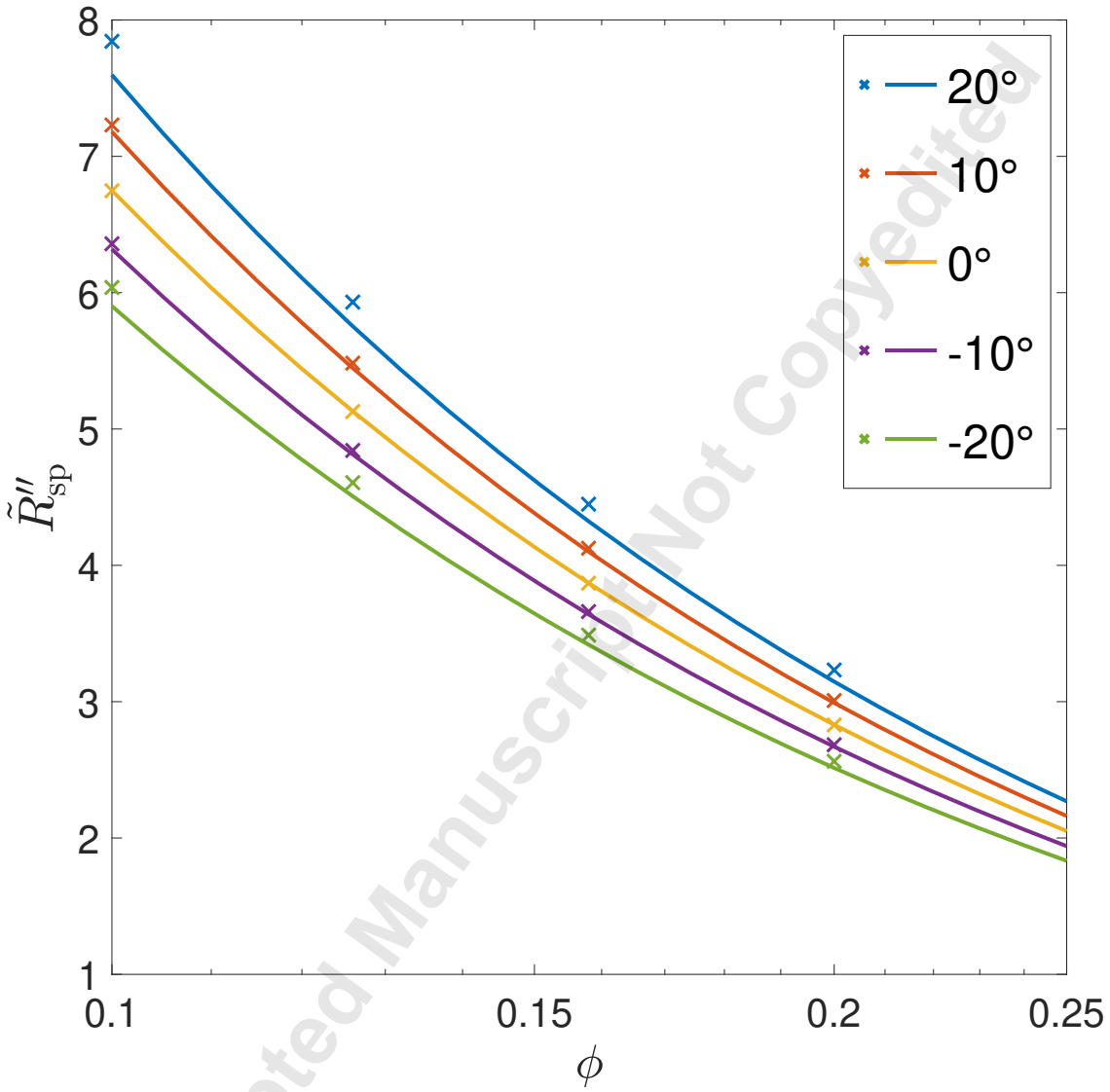


Figure 10: Dimensionless spreading resistance (solid lines) and numerical results (x) for range of constriction ratio and contact angle of typical real contacts.

Accepted Manuscript Not Copyedited

Downloaded From: https://heattransfer.asmedigitalcollection.asme.org on 01/28/2019 Terms of Use: http://www.asme.org/about-asme/terms-of-use

Journal of Heat Transfer. Received July 24, 2018;
Accepted manuscript posted January 08, 2019. doi:10.1115/1.4042441
Copyright (c) 2019 by ASME

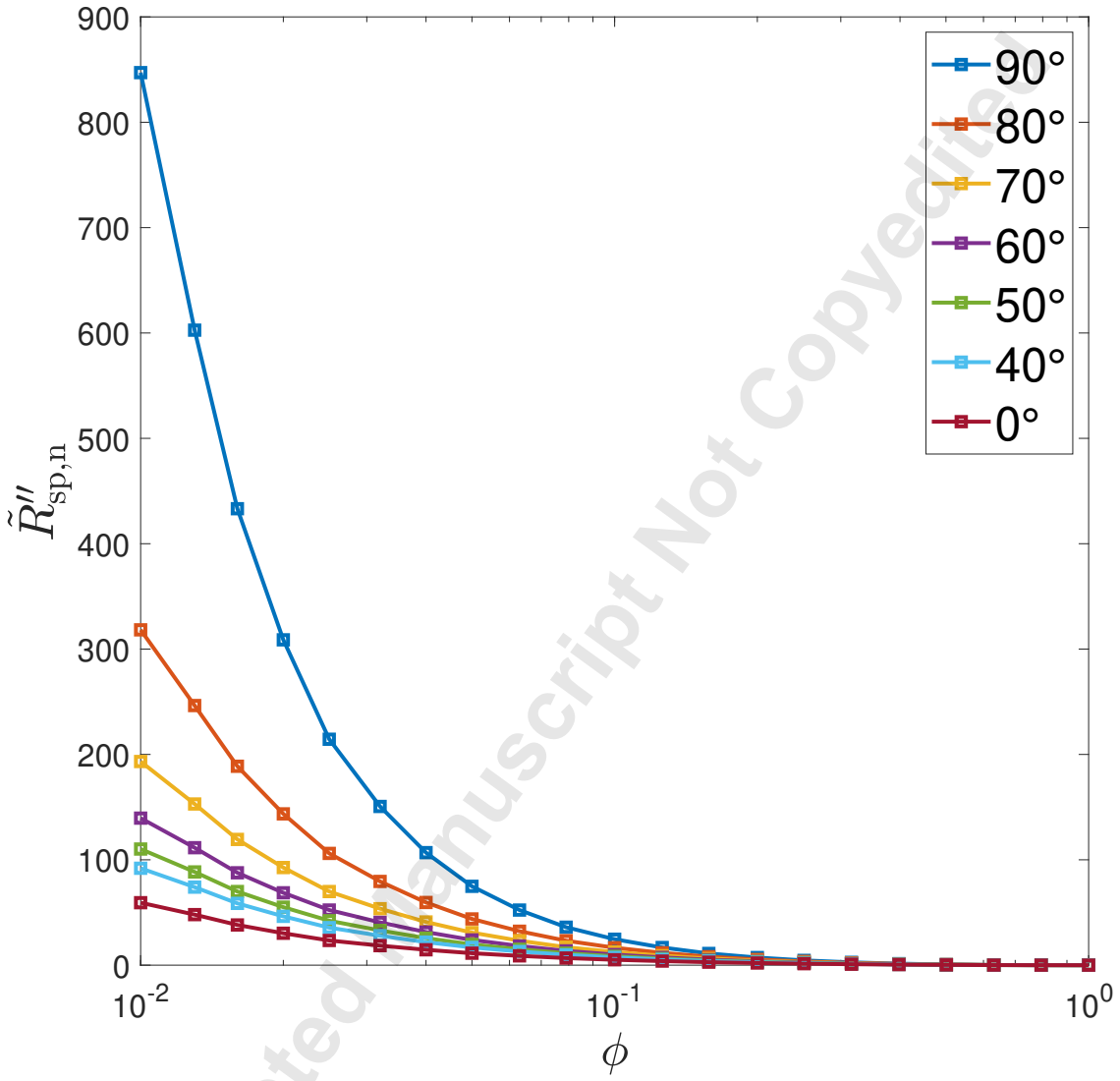


Figure 11: Dimensionless spreading resistance calculated numerically for contact angles higher than 40 degrees.

Accepted Manuscript Not Copyedited

Downloaded From: https://heattransfer.asmedigitalcollection.asme.org on 01/28/2019 Terms of Use: http://www.asme.org/about-asme/terms-of-use

Journal of Heat Transfer. Received July 24, 2018;
Accepted manuscript posted January 08, 2019. doi:10.1115/1.4042441
Copyright (c) 2019 by ASME

$\tilde{R}''_{\mathrm{sp,n}}$ as $\phi \to 0$. Figure 12 shows dimensionless spreading resistance for contact angles from -40 degrees to -90 degrees, showing a significant alleviation of spreading resistance at large negative angles due to the increase in overall volume available for heat transfer as illustrated in Fig. 6d). Additionally, comparison of Figs. 11 and 12 reveals that the decrease in spreading resistance caused by negative contact angles is less than the increase in spreading resistance caused by positive contact angles of the same magnitude. This is consistent with our reasoning for why the asymptotic analysis underestimates spreading resistance for negative contact angles.

6 Singularity Analysis

Kirk *et al.* [22] and Game *et al.* [23] used local analyses in Cartesian problems with similar geometries and boundary conditions to investigate the singularity in the partial derivative of temperature that arises due to the mixed boundary condition at $(\phi, 0)$. We do the same to look at the convergence of the series solution for the flat-contact problem and to ensure the expected singularity behavior is captured by the FEA. The analytical solutions in our paper are based on truncating infinite series at $n = N$ as is sufficient for the series to converge. The rate of convergence depends on the decay of each term in the summation and is related to the strength of the singularity in the derivative of the temperature field due to the mixed-boundary condition. All terms in the flat-base temperature field decay exponentially for $\tilde{z} > 0$; however, at $\tilde{z} = 0$, the decay becomes algebraic and a local analysis can be used to reveal the type of singularity at $\tilde{r} = \phi$.

To center the local analysis at $(\phi, 0)$ we introduce new variables r' and z' defined by $\tilde{r} = \phi + \delta r'$ and $\tilde{z} = \delta z'$,where $\delta \ll 1$. Laplace's Equation in axisymmetric cylindrical coordinates is

$$\frac{1}{\tilde{r}} \frac{\partial}{\partial \tilde{r}} \left(\tilde{r} \frac{\partial \tilde{T}}{\partial \tilde{r}} \right) + \frac{\partial^2 \tilde{T}}{\partial \tilde{z}^2} = 0 \tag{60}$$

Plugging in for $\tilde{r}, \tilde{z}$ and keeping only the leading-order terms in δ yields

$$\frac{\partial^2 \tilde{T}}{\partial r'^2} + \frac{\partial^2 \tilde{T}}{\partial z'^2} = 0 \tag{61}$$

the Laplace Equation in Cartesian coordinates. Correspondingly, in the local problem the adiabatic arc becomes a straight line as per

$$z' = \tan(\alpha) r' \tag{62}$$

To more easily solve this problem, we transform to polar coordinates (ρ, ψ) centered at $(r', z') = (0, 0)$, where ρ is the radial coordinate and ψ is the azimuthal one with the clockwise direction as positive. The isothermal condition on the contact spot is given by $\tilde{T}(\rho, 0) = 1$ for $\rho > 0$. The adiabatic condition along the tangent line is given by $\partial \tilde{T} / \partial \psi|_{\psi = \pi - \alpha} = 0$. The problem takes the form of a wedge, as depicted in Fig. 13.

We define $\tilde{T} = 1 + \tilde{T}_{\mathrm{local}}$, where 1 is the particular solution that satisfies the inhomogeneous boundary condition at $\psi = 0$ and $\tilde{T}_{\mathrm{local}}$ is the solution to the homogeneous problem. The solutions to Laplace's Equation in polar coordinates are

$$\left(A_n \rho^{\mu_n} + B_n \rho^{-\mu_n}\right) \left[\left(C_n \cos(\mu_n \psi) + D_n \sin(\mu_n \psi)\right)\right] \tag{63}$$

where μ_n are the eigenvalues and, A_n, B_n, C_n, and D_n are constants. Temperature in this region is not infinite; therefore, $B_n = 0$. Moreover, due to the isothermal condition on the contact spot, $C_n = 0$. The

Accepted Manuscript Not Copyedited

Downloaded From: https://heattransfer.asmedigitalcollection.asme.org on 01/28/2019 Terms of Use: http://www.asme.org/about-asme/terms-of-use

Journal of Heat Transfer. Received July 24, 2018;
Accepted manuscript posted January 08, 2019. doi:10.1115/1.4042441
Copyright (c) 2019 by ASME

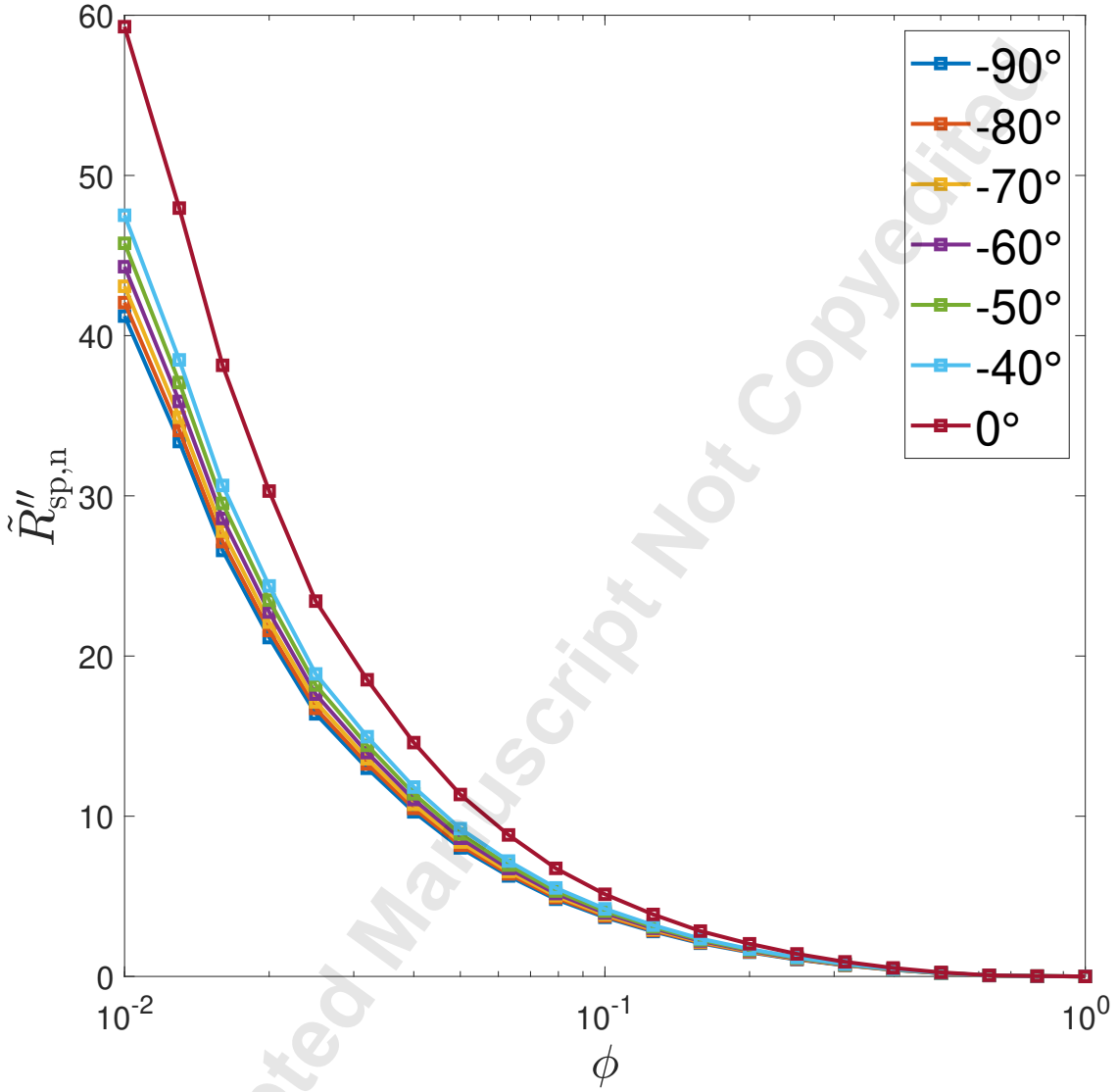


Figure 12: Dimensionless spreading resistance calculated numerically for contact angles less than negative 40 degrees.

Accepted Manuscript Not Copyedited

Downloaded From: https://heattransfer.asmedigitalcollection.asme.org on 01/28/2019 Terms of Use: http://www.asme.org/about-asme/terms-of-use

Journal of Heat Transfer. Received July 24, 2018;
Accepted manuscript posted January 08, 2019. doi:10.1115/1.4042441
Copyright (c) 2019 by ASME

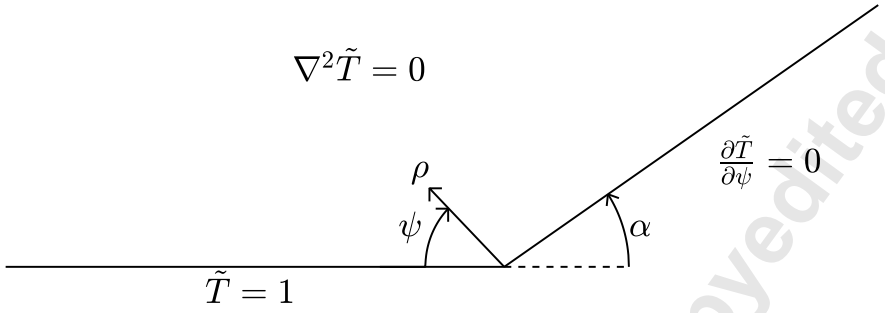


Figure 13: Domain of local analysis

eigencondition is given by the adiabatic boundary condition on the tangent line as $\mu_n(\pi - \alpha\pi/180°) = \pi/2 + n\pi$. The most singular part occurs at $n = 0$ and as this solution dominates the singularity behavior [23] we take

$$\tilde{T}_{\text{local}} \sim \rho^{\mu_0} \sin(\mu_0 \psi) \tag{64}$$

where $\mu_0 = \pi/[2(\pi - \alpha\pi/180°)]$ when $n = 0$.

Equation (64) shows a square root singularity in the derivative for the flat-contact problem, i.e., that $\tilde{T}_0(\tilde{r}, 0) = O(|\tilde{r} - \phi|^{1/2})$, as $\tilde{r} \to \phi^+$. For large n, λ_n satisfying $J_1(\lambda_n) = 0$ are known [24, 25] and are given by

$$\lambda_n = n\pi + \frac{\pi}{4} - \frac{3}{8n\pi + 2\pi} + O\left(\frac{1}{n^3}\right) \tag{65}$$

such that $\lambda_n = O(n)$ as $n \to \infty$. Since it is also known that $J_0(\lambda_n \tilde{r}) = O(n^{-1/2})$ as $n \to \infty$ and that $C_n = O(1)$ as confirmed by Fig. 14, then $C_n \lambda_n^{-1} J_0(\lambda_n \tilde{r}) = O(n^{-3/2})$. Thus, as $n \to \infty$ the series in Eq. (28) decays like a Fourier series with a square root singularity [22]. This validates our choice of $N = 1500$.

Additionally, we can use the local analysis solution for non-zero contact angle to verify that the FEA captures the correct singularity behavior at $(\phi, 0)$. The singularity on the contact spot arises in the partial derivative with respect to $\tilde{z}$, i.e.,

$$\left.\frac{\partial \tilde{T}}{\partial \tilde{z}}\right|_{\tilde{z}=0} = \frac{1}{\delta} \left.\frac{\partial \tilde{T}}{\partial z'}\right|_{z'=0} \tag{66}$$

which in local polar coordinates (ρ, ψ) becomes

$$\frac{1}{\delta} \left.\frac{\partial \tilde{T}}{\partial z'}\right|_{z'=0} \sim \frac{1}{\delta} \frac{1}{\rho} \left.\frac{\partial \tilde{T}}{\partial \psi}\right|_{\psi=0} \tag{67}$$

Accepted Manuscript Not Copyedited

Downloaded From: https://heattransfer.asmedigitalcollection.asme.org on 01/28/2019 Terms of Use: http://www.asme.org/about-asme/terms-of-use

Journal of Heat Transfer. Received July 24, 2018;
Accepted manuscript posted January 08, 2019. doi:10.1115/1.4042441
Copyright (c) 2019 by ASME

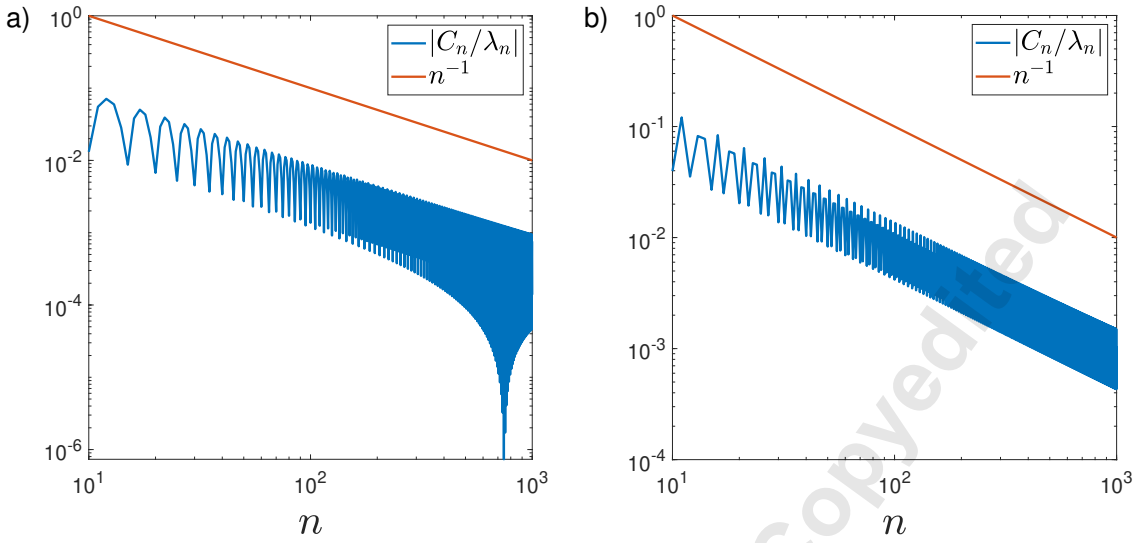


Figure 14: Decay rates of coefficients $C_n\lambda_n^{-1}$ as $n \to \infty$ for a) $\phi = 0.2$ and b) $\phi = 0.4$.

Substituting $\tilde{T} = 1+\tilde{T}_{\text{local}}$, where $\tilde{T}_{\text{local}}$ is given to within a multiplicative constant by Eq. (64) and evaluating the partial derivative on the contact spot, we get

$$\left.\frac{\partial \tilde{T}}{\partial \tilde{z}}\right|_{\tilde{z}=0} = O(\rho^{\mu_0-1}) \tag{68}$$

Plugging in for ρ,

$$\left.\frac{\partial \tilde{T}}{\partial \tilde{z}}\right|_{\tilde{z}=0} = O(|\phi-\tilde{r}|^{\mu_0-1}) \tag{69}$$

For local behavior,

$$\left.\frac{\partial \tilde{T}}{\partial \tilde{z}}\right|_{\tilde{z}=0} = A|\phi-\tilde{r}|^{\mu_0-1} \tag{70}$$

where A is a constant. Taking the logarithm results in

$$\log\left(\left.\frac{\partial \tilde{T}}{\partial \tilde{z}}\right|_{\tilde{z}=0}\right) = \log A + (1-\mu_0)\log\left(\frac{1}{\phi-\tilde{r}}\right) \tag{71}$$

To confirm that the FEA captured the correct behavior of the singularity, we plot $\log(\partial\tilde{T}_{\text{n}}/\partial\tilde{z})$ against $\log|1/(\phi-\tilde{r})|$. Then as $\tilde{r}\to\phi^-$, $\log(\partial\tilde{T}_{\text{n}}/\partial\tilde{z})$ should asymptote to a straight line with slope $1-\mu_0$ where, again, $\mu_0(\alpha) = \pi/[2(\pi-\alpha\pi/180°)]$. This behavior is verified by Fig. 15 for α ranging from 0° to 90° and $0.01 < \phi < 0.316$. We see agreement for all contact angles as $\log|1/(\phi-\tilde{r})|\to\infty$. Of note, the red lines in Fig. 15a-d) depict the case when $\alpha = 90°$, which the local analysis suggests does not have a singularity. This is supported by the constancy of the dimensionless numerical gradient for $\alpha = 90°$ as $\tilde{r}\to\phi^-$. Furthermore, we see an increase in the singularity as α decreases, consistent with the local analysis. Importantly, Fig. 15 confirms the FEA correctly captured the singularity behavior at $(\phi, 0)$.

Accepted Manuscript Not Copyedited

Downloaded From: https://heattransfer.asmedigitalcollection.asme.org on 01/28/2019 Terms of Use: http://www.asme.org/about-asme/terms-of-use

Journal of Heat Transfer. Received July 24, 2018;
Accepted manuscript posted January 08, 2019. doi:10.1115/1.4042441
Copyright (c) 2019 by ASME

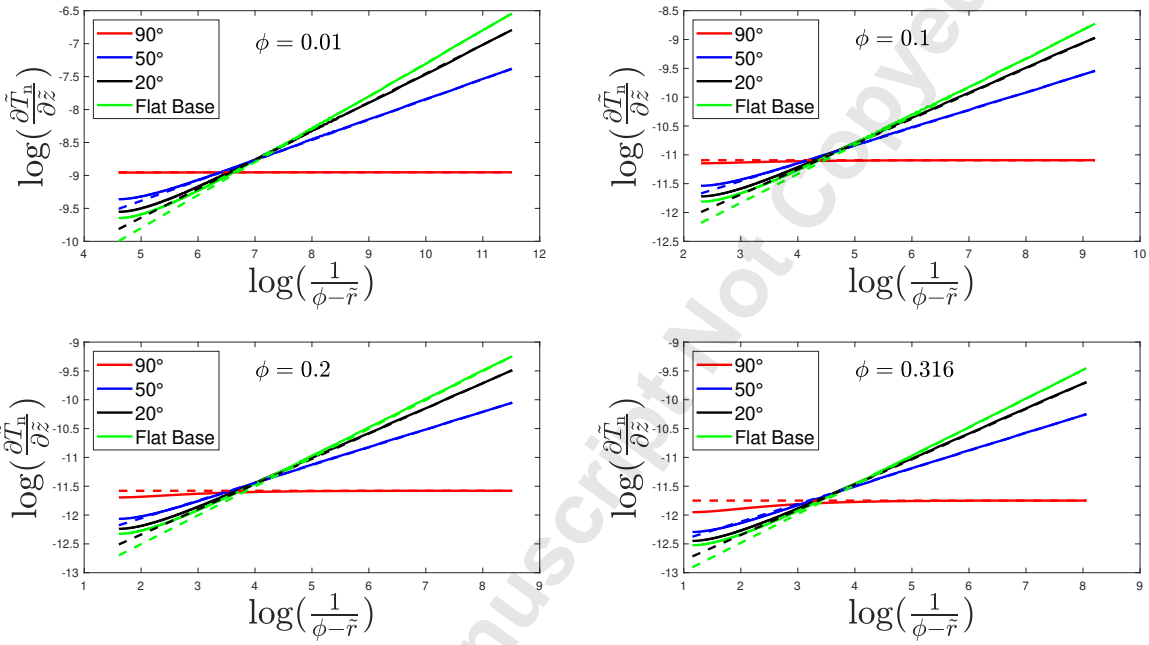


Figure 15: Log-log plot of numerical gradient at $\tilde{z} = 0$ as $r \to \phi^-$ for $\phi = 0.01,\ 0.1,\ 0.2,\ 0.316$ and various values of α chosen to span the range of positive values of α. The dotted lines are lines with slope $1 - \mu_0(\alpha)$ for the values of α depicted in the legend.

Accepted Manuscript Not Copyedited

Downloaded From: https://heattransfer.asmedigitalcollection.asme.org on 01/28/2019 Terms of Use: http://www.asme.org/about-asme/terms-of-use

Journal of Heat Transfer. Received July 24, 2018;
Accepted manuscript posted January 08, 2019. doi:10.1115/1.4042441
Copyright (c) 2019 by ASME

7 Conclusions

We have developed analytical thermal spreading expressions for a single, isothermal, circular contact for contact geometries accounting for the non-flat nature of real contacts. By using reciprocity arguments, we solved them with only knowledge of the temperature field in a flat contact, a known quantity in the literature. The analytical model is applicable for a range of small protrusion angles and constriction ratios which are typical of contact geometries generated between contacting materials after machining [7, 26]. Our model shows that small perturbations from a flat contact can have significant effects on spreading resistance, which is readily converted to contact resistance. Importantly, the non-flatness of contacts has the most significant effect on contact resistance at lower constriction ratios relevant to real surfaces. In addition, we conducted an FEA that validated our analytical results for small contact angle and constriction ratios. We used the numerical simulation to complete the parameter space, evaluating spreading resistance for arbitrary contact angles and constriction ratios. By performing a local analysis we were able to show that the FEA correctly captured the singularity in the derivative at the edge of the contact spot. For practical purposes, since constriction ratios and contact angles follow from knowledge of asperity heights and slopes, parameters already used in existing models for contact resistance, our expressions can be easily implemented into existing models to allow for better estimates of it. Further work is needed to include the presence of a conducting fluid in the gap, as well as to determine the effect of interactions between neighboring contacts on the overall contact resistance. Additionally, work is needed to perform this analysis where the isothermal boundary condition on the contact spot is replaced by an isoflux boundary condition, which is known to significantly change spreading resistance [27]. We note that one can use our model to perform this analysis for different contact geometries such as the convex shape illustrated in Fig. 4c).

8 Acknowledgments

The computations in this paper were run on the Tufts High-performance Computing Research Cluster at Tufts University. M. Mayer was supported by NSF IGERT: Soft Material Robotics program under award DGE-1145591. M. Hodes was supported in part by NSF CBET award 1402783. T. L. Kirk was supported by an EPSRC Doctoral Prize Fellowship. D. Crowdy is supported by an EPSRC Established Career Fellowship (EP/K019430/10) and by a Royal Society Wolfson Research Merit Award.

Accepted Manuscript Not Copyedited

Downloaded From: https://heattransfer.asmedigitalcollection.asme.org on 01/28/2019 Terms of Use: http://www.asme.org/about-asme/terms-of-use

Journal of Heat Transfer. Received July 24, 2018;
Accepted manuscript posted January 08, 2019. doi:10.1115/1.4042441
Copyright (c) 2019 by ASME

References

[1] B. B. Mikic and W. M. Rohsenow, "Thermal contact resistance," Tech. Rep. September, MIT, 1966.

[2] M. Yovanovich and E. Marotta, "Thermal spreading and contact resistances," in *Handboook of Heat Transfer* (A. Bejan and A. Kraus, eds.), pp. 261,393, Wiley, 2003.

[3] D. G. Crowdy, "Analytical formulae for longitudinal slip lengths over unidirectional superhydrophobic surfaces with curved menisci," *Journal of Fluid Mechanics*, vol. 791, 2016.

[4] M. Hodes, T. Kirk, and D. Crowdy, "Spreading and Contact Resistance Formulae Capturing Boundary Curvature and Contact Distribution Effects," *Journal of Heat Transfer*, no. 2, 2018.

[5] M. G. Cooper, B. B. Mikic, and M. M. Yovanovich, "Thermal Contact Conductance," *Int. J. Heat Mass Transer*, vol. 12, pp. 279–300, 1969.

[6] A. K. Das and S. S. Sadhal, "The Effect of Interstitial Fluid on Thermal Constriction Resistance," *Journal of Heat Transfer*, vol. 114, p. 1045, nov 1992.

[7] K. Negus and M. Yovanovich, "Constriction Resistance of Circular Flux Tubes with Mixed Boundary Conditions by Linear Superposition of Neumann Solutions," *ASME Paper 84-HT-84*, pp. 1–6, 1984.

[8] A. Hunter and A. Williams, "Heat Flow Across Metallic Joints - The Constriction Alleviation Factor," *Int. J. Heat Mass Transer*, vol. 12, pp. 524–526, 1968.

[9] I. N. Sneddon, *Mixed Boundary Value Problems in Potential Theory.* Amsterdam: North-Holland Publishing Company, 1966.

[10] J. A. Greenwood and J. B. P. Williamson, "Contact of Nominally Flat Surfaces," *Proceedings of the Royal Society A: Mathematical, Physical and Engineering Sciences*, vol. 295, no. 1442, pp. 300–319, 1966.

[11] M. M. Yovanovich, "Four decades of research on thermal contact, gap, and joint resistance in microelectronics," *IEEE Transactions on Components and Packaging Technologies*, vol. 28, pp. 182–206, jun 2005.

[12] M. Razavi, Y. S. Muzychka, and S. Kocabiyik, "Review of Advances in Thermal Spreading Resistance Problems," *Journal of Thermophysics and Heat Transfer*, vol. 30, no. 4, pp. 863–879, 2016.

[13] C. V. Madhusudana, "Heat Flow Through Conical Constrictions," *AIAA Journal*, vol. 18, no. 10, pp. 1261–1262, 1980.

[14] Y. Sano, "Effect of space angle on constriction resistance and contact resistance for a point contact," *Journal of Applied Physics*, vol. 58, no. 7, pp. 2651–2654, 1985.

[15] A. K. Das, *Thermal Constriction Resistance: Effects of Clustering, Random Distribution and Interstitial Fluid.* Phd thesis, University of Southern California, 1994.

[16] A. K. Das and S. S. Sadhal, "Analytical solution for constriction resistance with interstitial fluid in the gap," *Heat and Mass Transfer*, vol. 34, no. 2-3, pp. 111–119, 1998.

Accepted Manuscript Not Copyedited

Downloaded From: https://heattransfer.asmedigitalcollection.asme.org on 01/28/2019 Terms of Use: http://www.asme.org/about-asme/terms-of-use

Journal of Heat Transfer. Received July 24, 2018;
Accepted manuscript posted January 08, 2019. doi:10.1115/1.4042441
Copyright (c) 2019 by ASME

[17] R. Enright, M. Hodes, T. Salamon, and Y. Muzychka, "Isoflux Nusselt Number and Slip Length Formulae for Superhydrophobic Microchannels," *Journal of Heat Transfer*, vol. 136, no. 1, p. 012402, 2013.

[18] M. Sbragaglia and A. Prosperetti, "A note on the effective slip properties for microchannel flows with ultrahydrophobic surfaces," *Physics of Fluids*, vol. 19, no. 4, pp. 1–8, 2007.

[19] L. Steigerwalt Lam, M. Hodes, G. Karamanis, T. Kirk, and S. MacLachlan, "Effect of Meniscus Curvature on Apparent Thermal Slip," *Journal of Heat Transfer*, vol. 138, no. 12, p. 122004, 2016.

[20] D. G. Crowdy, "Perturbation analysis of subphase gas and meniscus curvature effects for longitudinal flows over superhydrophobic surfaces," *Journal of Fluid Mechanics*, vol. 822, no. 19, pp. 307–326, 2017.

[21] Michael Mayer, *Effect of Surface Curvature on Contact Resistance between Abutting Cylinders*. PhD thesis, Tufts University, 2018.

[22] T. L. Kirk, M. Hodes, and D. T. Papageorgiou, "Nusselt numbers for Poiseuille flow over isoflux parallel ridges accounting for meniscus curvature," *Journal of Fluid Mechanics*, vol. 811, pp. 315–349, 2017.

[23] S. Game, T. L. Kirk, M. Hodes, and D. T. Papageorgiou, "Nusselt numbers for Poiseuille flow over isoflux parallel ridges for arbitray meniscus curvature," *Journal of Fluid Mechanics*, vol. 811, no. August, pp. 315–349, 2017.

[24] G. Watson, *A Treatise on the Theory of Bessel Functions*. London: Cambridge University Press, 2nd ed., 1966.

[25] Á. Elbert, "Some recent results on the zeros of Bessel functions and orthogonal polynomials," *Journal of Computational and Applied Mathematics*, vol. 133, no. 1-2, pp. 65–83, 2001.

[26] A. Grigoriev, "Slope angles of rough surface asperities after machining," *Journal of Friction and Wear*, vol. 36, no. 3, pp. 197–199, 2015.

[27] H. Carslaw and J. Jaeger, *Conduction of Heat in Solids*. Oxford: Clarendon Press, 2nd editio ed., 1959.

Accepted Manuscript Not Copyedited

Downloaded From: https://heattransfer.asmedigitalcollection.asme.org on 01/28/2019 Terms of Use: http://www.asme.org/about-asme/terms-of-use